energies

MDPI

Article

Performance Analysis of Eco-Friendly Binary Organic Working Fluids for a Medium-Temperature Geothermal-Driven Organic Rankine Cycle

Mehmet Özçelik

Department of Mechanical Engineering, Faculty of Engineering, Van Yuzuncu Yil University, Van 65080, Türkiye; mehmetozcelik@yyu.edu.tr; Tel.: +90-(432)-225-17-27 (ext. 28282)

Abstract

Energy and exergy analyses of a geothermal-driven Organic Rankine Cycle (ORC) utilizing alternative organic mixtures with low global warming potential (GWP) as working fluids were conducted. New mixtures were created in REFPROP 10 using organic fluids commonly employed in fluid analysis. Among the 108 newly formulated organic working fluid mixtures, 12 candidates characterized by a temperature glide of less than 5 °C, a high critical temperature, and a GWP value below 750 were selected for this study. Energy and exergy assessments were performed for power generation using the selected fluids at geothermal brine temperatures of 130–150 °C (in 5 °C increments) and a condenser temperature of 30 °C. Additionally, the cycle's net power output ($\dot{W}_{net}$), thermal efficiency (η_{th}) and second-law efficiency (η_{II}) were quantified. Based on the simultaneous maximization of $\dot{W}_{net}$, η_{th} and η_{II} specific fluid recommendations are proposed: b7 is optimal for low-temperature, ultra-low-GWP geothermal and waste heat conversation (GWP < 150, T_{CR} < 165 °C); b1 is recommended for high-enthalpy geothermal applications requiring low environmental impact (GWP < 150, T_{CR} > 165 °C); and b9 serves as the prime candidate for medium-GWP (150 < GWP < 750) commercial power plants aiming for maximum energy conversation. Among all evaluated working fluids, b7 (GWP < 150) achieved the maximum $\dot{W}_{net}$, η_{th} and η_{ii}, proving to be the most promising organic blend owing to its favorable thermophysical properties and ultra-low GWP.

Keywords: alternative organic blend; electricity generation; energy efficiency; exergy efficiency; GWP; Organic Rankine cycle

Check for updates

Academic Editor: Francesco Calise

Received: 25 October 2026
Revised: 18 November 2026
Accepted: 20 November 2026
Published: 26 November 2026

Copyright: © 2026 by the author. Licensee MDPI, Basel, Switzerland. This article is an open access article distributed under the terms and conditions of the Creative Commons Attribution (CC BY) license.

1. Introduction

In the modern global landscape, energy constitutes a cornerstone driving the economic development and societal advancement of nations worldwide [1].

The alarming escalation of environmental degradation caused by fossil fuel consumption, coupled with the accelerating global energy demand, renders the transition toward sustainable energy conversation infrastructures imperative. Furthermore, energy consumption is expanding rapidly in tandem with economic growth, thereby intensifying greenhouse gas emissions and exacerbating global warming [2]. The continuous rise in energy consumption, air pollution, global warming, and greenhouse gas effects has inevitably driven the search for alternative energy solutions. Within the spectrum of renewable energy systems, solar and wind installations have exhibited the most rapid expansion, jointly constituting the vast majority of recent additions to worldwide electricity generation [3]. Concurrently,

geothermal energy has garnered mounting interest as a renewable alternative, owing to its baseload capability, uninterrupted availability, and independence from meteorological fluctuations [4,5]. Organic Rankine Cycles (ORCs) are extensively deployed on a commercial scale to generate power from low-to-medium-temperature heat sources, predominantly in geothermal power plants, industrial waste heat recovery (WHR) systems, and biomass cogeneration facilities. In addition, they are widely recognized as an efficient thermodynamic conversation solution in emerging renewable applications, such as concentrated solar power (CSP) systems and ocean thermal energy conversation (OTEC). In contrast to standard Rankine Cycles (RC), which operate with water, ORCs utilize organic working fluids to generate electricity from the thermal energy extracted from a heat source.

Geothermal waters typically reside at low-to-medium enthalpy levels (80–180 °C), thereby exhibiting poor thermodynamic performance in conventional steam Rankine Cycles (RCs); however, they can be efficiently converted into electrical power with high thermal and exergy efficiencies via ORCs utilizing organic fluids characterized by low boiling points, high molecular weights, and dry or isentropic expansion behaviors. Furthermore, the weather-independent, continuous, and steady thermal input inherent to geothermal reservoirs preserves an optimal temperature profile match (minimizing pinch-point temperature differences and local irreversibilities) during phase change in the evaporator, thereby maximizing the thermo-economic feasibility of the system.

In the open literature, numerous studies have investigated Organic Rankine Cycles (ORCs) driven by waste heat and geothermal energy, as well as their integration into combined power cycle configurations [6–12]. Ortega-Sarceda and Arce analyzed and optimized energy recovery from medium-temperature waste heat sources using regenerative ORC (R-ORC) and reheat-regenerative ORC (RR-ORC) configurations, evaluated with and without superheating. Ten distinct working fluids, namely R1234ze(Z), butane, cis-butene, trans-butene, isobutane, pentane, isopentane, R245fa, R1336mzz(Z), and R1233zd(E), were selected based on their thermodynamic and safety profiles. Key operational conditions were optimized via the Particle Swarm Optimization (PSO) algorithm to maximize thermal efficiency for each cycle architecture and working fluid. When employing trans-butene with superheating, the highest thermal efficiencies reached 17.64% for the R-ORC and 19.78% for the RR-ORC. In the absence of superheating, peak thermal efficiencies were recorded as 12.22% for the R-ORC (using isopentane) and 17.67% for the RR-ORC (using pentane). The combined implementation of superheating and reheating was demonstrated to enhance both the thermal efficiency and net power output of the regenerative cycle [13].

Cogeneration, defined as the simultaneous generation of electricity and heat, has gained increasing prominence for improving overall energy utilization and efficiency. Safari et al. investigated a cogeneration system integrated with a cascade Organic Rankine Cycle (CORC) designed to deliver auxiliary power support and thermal management. The high- and low-temperature stages of the cascade cycle utilized R227ea and R116 as working fluids, respectively. The system's electrical power output, thermal energy delivery, and overall efficiency were comprehensively evaluated. According to their investigation, electrical outputs of around 31 MW and 4 MW were achieved by the CHP configuration and the cascade ORC, respectively, alongside a joint heating capacity of 181 MW and an overall thermal efficiency of nearly 87% [14].

For a combined ORC and Auto-Refrigerating Cascade (ARC) architecture powered by low-grade thermal energy, a zeotropic blend of R170/R290 was employed in the ARC stage, while dry organic fluids including R245fa, R245ca, RE245cb2, RE245fa2, R1224yd(Z), R1233zd(E), and R1336mzz(Z) were selected for the ORC power loop. In their study, the researchers performed a parametric investigation using a comprehensive thermodynamic model to evaluate the influence of condensation and evaporation parameters on overall

system behavior. The study highlights the feasibility of exploiting low-temperature renewable energy sources to attain ultra-low temperatures, thereby establishing a benchmark for future research on the proposed architecture. The operational coefficient of performance (COP) was reported to range between 3.8 and approximately 20 across all investigated scenarios. In another study comparing distinct ORC configurations, a double-flash geothermal power plant integrated with an ORC was proposed, where the ORC unit served to recover waste heat and enhance overall plant efficiency. To evaluate energy and exergy efficiencies alongside ecological indicators, specifically ozone depletion potential (ODP) and global warming potential (GWP), several working fluids such as R245fa, R600, and R452a were analyzed. Incorporating an ORC markedly enhanced thermodynamic performance relative to the standalone geothermal setup, yielding gains of up to 512% in net power generation and 22% in energy efficiency. Among the tested fluids, R245fa and R600 proved to be the most effective options, attaining peak energy efficiencies of 15.67% and 15.5% and exergy efficiencies of 61.4% and 60.79%, respectively, with minimal exergy destruction [15,16].

A comparative energy and exergy assessment was carried out for basic, reheat, and regenerative ORC configurations utilizing ultra-low-GWP fluids (GWP < 10). To evaluate the thermodynamic viability of six candidate refrigerants, R1243zf, R1234yf, R1234ze(E), R1224yd(Z), R1233zd(E), and R1336mzz(Z), a numerical simulation tool developed in Python was used to solve governing mass, energy, entropy, and exergy balances. The parametric evaluation focused on the sensitivities of net power generation, thermal and exergy efficiencies, and overall exergy destruction to variations in turbine inlet pressure (1–2.5 MPa) and pump inlet pressure (0.8–2 MPa). The outcomes demonstrated that R1243zf consistently exhibited the highest performance across all investigated cycle architectures, followed in descending order by R1234yf, R1234ze(E), R1224yd(Z), R1233zd(E), and R1336mzz(Z). Given that environmental policies restrict refrigerants with a GWP exceeding 150 and zeotropic blends are well-established for enhancing ORC exergy efficiency, researchers have evaluated binary mixtures combining R32 with eight ultra-low GWP fluids (n-pentane, NOVEC649, R1233zd, isobutane, R1234ze, R1234yf, propylene, and CO2) across both basic and recuperative ORC layouts. By optimizing evaporation pressure alongside component molar fractions, their analysis revealed an inverse relationship between heat source temperature and the relative exergy efficiency gain of zeotropic ORCs (ZORCs) over pure-fluid ORCs (PORCs), declining from a peak of 36.39% at 100 °C to under 5% above 200 °C. Overall, ZORCs outperformed their pure counterparts by an average of roughly 30–50%, proving particularly advantageous when heat source temperatures lie primarily below, or secondarily between, the critical temperatures of the constituent fluids. As heat source temperatures rise, ZORCs utilizing isobutane, NOVEC649, R1233zd, and n-pentane emerge as sequentially optimal. Furthermore, an energy and exergy comparison was conducted on a single-flash geothermal-ORC trigeneration layout incorporating a self-superheater (SSH), evaluating four arrangements with and without the SSH operating with R245fa and the low-GWP alternative R1233zd(E) under identical boundary conditions. R1233zd(E) demonstrated superior performance over R245fa across all scenarios, elevating the energy utilization factor from 0.6137 to 0.6209 and exergy efficiency from 0.6231 to 0.6449 in the baseline layout, while reaching 0.6161 and 0.6472 when the SSH was integrated. Additionally, incorporating the SSH boosted net power generation from 9460 to 9514 kW for R245fa and from 9836 to 9895 kW for R1233zd(E), alongside corresponding cooling capacity gains from 3806 to 3855 kW and from 3850 to 3900 kW. These enhancements were offset by a minor drop in heating exergy from 1229 to 1207 kW across both fluids, leaving the SSH-integrated R1233zd(E) arrangement as the top performer with 9895 kW of net power, 3900 kW of cooling capacity, and an exergy efficiency of 0.6472. Meanwhile, pairing energy assessments with exergy analysis has gained substantial traction for pinpointing sources

of irreversibility and exergy destruction in thermal systems, particularly as environmental pressures drive interest in recovering low-grade waste heat via ORCs. In a Python-based comparative simulation of basic and regenerative ORC architectures using low-GWP and low-ODP refrigerants, specifically R1233zd(E), R1234ze(Z), R1234ze(E), and R1234yf, the regenerative configuration exhibited superior first- and second-law efficiencies alongside reduced exergy destruction. Fluids possessing higher critical temperatures consistently yielded better thermodynamic outcomes, with R1233zd(E) outperforming the other eco-friendly candidates in both cycle layouts. Although R1233zd(E) trailed the environmentally harmful R113 in second-law efficiency by 1–5.66% in the regenerative cycle and up to 4.17% in the basic cycle, it serves as a viable, sustainable substitute with only a marginal efficiency trade-off [17–20].

Thermal extraction from geothermal resources, power generation via ORCs, and mixture-based ORC configurations have been widely explored in the open literature. Focusing on a retrofitted abandoned well in a high-temperature reservoir at the Riau oilfield in Indonesia, researchers developed a validated, coupled transient ground-wellbore model integrated with an ORC simulator to assess geothermal power viability over a 20-year lifespan. Water served as the downhole heat carrier, while R245fa was utilized in the ORC power block. Evaluated design parameters encompassed the ORC pump frequency, expander speed, brine circulation rate, and well casing insulation length. Under standard baseline conditions, a 3 km limestone formation featuring a geothermal gradient of 0.04 °C/m, injecting water at 70 °C with a mass flow rate of 1.5 kg/s, transferred more than 72 kW of thermal energy to the ORC, yielding 6.3 kW of electrical output. Subsequent parametric optimization of the wellbore and ORC operational parameters demonstrated that daily electrical yields could be expanded from 151.2 kWh to roughly 250 kWh [21].

Aiming to improve the thermal stability of the low-GWP refrigerant R1243zf in medium to high-temperature ORC applications, researchers systematically examined the pyrolysis characteristics of a zeotropic R1243zf/CO_2 blend along with the suppressive role of CO_2 during thermal decomposition. By combining experimental testing with reactive force field molecular dynamics (ReaxFF MD) simulations and Density Functional Theory (DFT) modeling in a multiscale framework, they clarified both the macroscopic stability gains and the governing microscopic reaction pathways. Notably, experimental measurements revealed that introducing CO2 raised the initial pyrolysis temperature from 180–200 °C for neat R1243zf to 240–260 °C for the binary mixture [22].

Aiming at the efficient utilization of hot dry rock reservoirs, a combined system designated as the flash cycle-modified dual-pressure Organic Rankine cycle (FC-MDPORC) integrating a flash cycle with a modified DPORC was developed, formulated, and validated. The thermodynamic influences of six organic fluids (R600, R600a, R601, R601a, cyclopentane, and R1233zd) were evaluated, identifying R1233zd as the most favorable candidate. The R1233zd-based layout was subsequently optimized via the PSO algorithm to maximize net power generation, after which its energy performance was compared against baseline architectures. Results demonstrated that the FC-MDPORC design enhanced thermal efficiency, exergy efficiency, and net power output by 17.2%, 17.8%, and 26.7%, respectively, compared to the FC-DPORC system [23].

Researchers have also explored the capacity of low-GWP hydrofluoroolefin/hydrocarbon (HFO/HC) zeotropic blends to function as a thermal buffer that boosts cumulative energy production under fluctuating heat input conditions. Because zeotropic mixtures undergo non-isothermal phase transitions characterized by temperature glide, they naturally accommodate time-varying heat source profiles better than pure substances. Optimizing the blend ratio through a quasi-steady-state model simulating a daily thermal cycle between 100 and 180 °C with the objective of maximizing total energy yield instead of peak instantaneous

output revealed that an optimal 88/12 wt% R1234yf/isobutane formulation ("Mixture ID 1") elevated total daily energy generation by 88.54% over the reference refrigerant R245fa. Complementing these numerical findings, an experimental investigation on a kW-scale ORC test rig assessed R134a/R245fa and R227ea/R245fa blends across varying heat source temperatures (HST) and mass fractions (MF), benchmarking them against pure fluids at equivalent working fluid charge levels. System performance improved consistently as HST rose and the R245fa proportion declined, peaking at 1.8 kW net power and 25.6% exergy efficiency for an equimolar (0.5/0.5) R134a/R245fa mixture at 100 °C HST, while an equimolar R227ea/R245fa blend attained the highest thermal efficiency of 6.1% at 120 °C HST [24,25].

While ORC performance is primarily governed by the heat source temperature, system operating parameters, and working fluid selection, the use of conventional refrigerants faces increasing regulatory restrictions. Specifically, regulations have banned the deliberate atmospheric release of F-gases, curtailed the utilization of high-GWP refrigerants, and instituted strict compliance requirements, including mandatory registration, labeling, and periodic leak checks [26].

Based on the premise that using a mixture as a working fluid could improve the output of a geothermal ORC, this study presents the modeling and thermodynamic analysis of an ORC system utilizing a geothermal heat source under steady-state operating conditions. The model was simulated using the Engineering Equation Solver (EES) software, with an eco-friendly fluid mixture, specifically R245fa/R600a in an appropriate molar ratio, employed as the working fluid. Under steady-state conditions, this mixture yielded superior results compared to using a pure working fluid. For the basic cycle, the system's energy efficiency, exergy efficiency, and net power output were 16.62%, 64.08%, and 2199 kW, respectively; for the regenerative cycle, these values were 20.72%, 67.76%, and 2326 kW, respectively [27]. Employing working fluid mixtures in ORC waste heat recovery (WHR) plants has been explored to enhance thermal profile matching between hot and cold streams in evaporators and condensers, thereby potentially elevating overall energy conversion efficiency. Building on this principle, researchers evaluated the thermodynamic, environmental (GWP), and operational safety (flammability) advantages of selecting optimal binary blends for air-cooled ORC bottoming units coupled with medium-scale industrial gas turbines. Comparing both simple recuperated and split-cycle architectures against a baseline combined cycle utilizing a cyclopentane-driven air-cooled recuperated ORC, their findings demonstrated that binary mixtures substantially broaden the range of viable working fluid candidates available to system designers [28]. Zeotropic working fluids are being extensively researched to enhance the performance of ORC's. In this study, an experimental investigation was conducted using a zeotropic mixture of R1234ze(E)/R245fa under specific operating conditions, and the operational behavior of the ORC system was evaluated. An ORC simulation model (BP-ORC) was developed, based on a back-propagation neural network and heat exchanger simulation modules. The underlying reasons for the observed variations in heat transfer and system performance among different working fluids were examined. The operational behavior of the heat exchangers and the system was simulated for operating conditions beyond those covered in the experimental study. Due to their relatively lower densities, R1234ze(E)/R245fa mixtures (in ratios of 0.25:0.75 and 0.50:0.50) allow for a wider operating range in terms of mass flow rate compared to R245fa. The R1234ze(E)/R245fa (0.50:0.50) mixture, benefiting from superior heat transfer performance, yields a 4.63% higher net power output than R245fa at a mass flow rate of 0.164 kg/s. Variations in density and operating pressure have a significant impact on heat transfer characteristics and overall system performance [29].

There are numerous studies in the literature—ranging from geothermal-assisted ORC systems and simple ORC configurations to more complex or combined ORC setups—that investigate the use of zeotropic mixtures as working fluids. These studies employ machine learning-based simulations to compare the performance of such mixtures against pure fluids. The primary objective of using these mixtures in ORC-based WHR plants is to improve the temperature profile alignment between the hot and cold fluids within the condenser and evaporator, thereby enhancing the system's energy conversion efficiency. These studies often include energy and exergy analyses, as well as thermo-economic evaluations, to assess the performance of binary mixtures at specific proportions under constant operating conditions.

In this study, a comprehensive investigation into geothermal-driven ORC power plants is presented. The energy and exergy performances of the ORC power plants were evaluated. For the ORC designed to produce electrical power from geothermal heat, candidate low-GWP working fluid blends were generated via REFPROP 10 in accordance with specific thermodynamic and environmental screening criteria. These 108 newly formulated organic fluid mixtures were evaluated within the mathematical model of the geothermal-driven Organic Rankine Cycle implemented in Engineering Equation Solver (EES) [30], from which the top 60 mixtures exhibiting superior η_{th} and η_{II} values were identified. Subsequently, mixtures exhibiting virtually identical η_{th} and η_{II} values were eliminated to avoid redundancy, thereby narrowing down the candidates to 12 optimal organic fluid mixtures selected as the working media for detailed cycle evaluation. The 12 selected organic blends were evaluated within the geothermal ORC framework modeled in EES, and the most favorable mixtures were identified based on the resulting thermodynamic indicators. Consequently, this study seeks to mitigate environmental degradation through low-GWP refrigerants while maximizing ORC thermodynamic performance. What uniquely sets this investigation apart from earlier studies is the systematic identification and evaluation of novel, tailor-made low-GWP organic fluid blends across varied thermal conditions and application scenarios.

2. Materials and Methods

2.1. Thermodynamic Cycle Description

In a conventional Rankine RC, water is utilized as the working fluid. The working fluid extracts heat from the thermal source in the evaporator, reaching a superheated vapor state at high temperature and pressure. Upon passing through the stationary turbine nozzles, it experiences an enthalpy drop that yields high kinetic energy. The high-speed flow then drives the rotating blades, translating the fluid's thermomechanical energy into shaft work. Finally, a synchronous generator directly coupled to the turbine shaft transforms this mechanical torque into electrical energy via electromagnetic induction and transmits it to the grid. Distinguished from the steam RC, the ORC operates with an organic working fluid. The layout of the thermodynamic system components of the geothermal-driven ORC is presented in Figure 1, and the cycle's T–s diagram is given in Figure 2.

The cycle consists of the following sequential stages:

1-2: Isentropic compression in the pump;

2-3: Constant-pressure heat input in the evaporator;

3-4: Isentropic expansion in the turbine;

4-1: Constant-pressure heat rejection in the condenser (Figures 1 and 2).

Figure 3 presents the *T-s* diagram for n-butane—one of the pure fluids used in the cycle—which is included here to facilitate a comparison with data for organic mixtures and to verify the validity of the hypothesis.

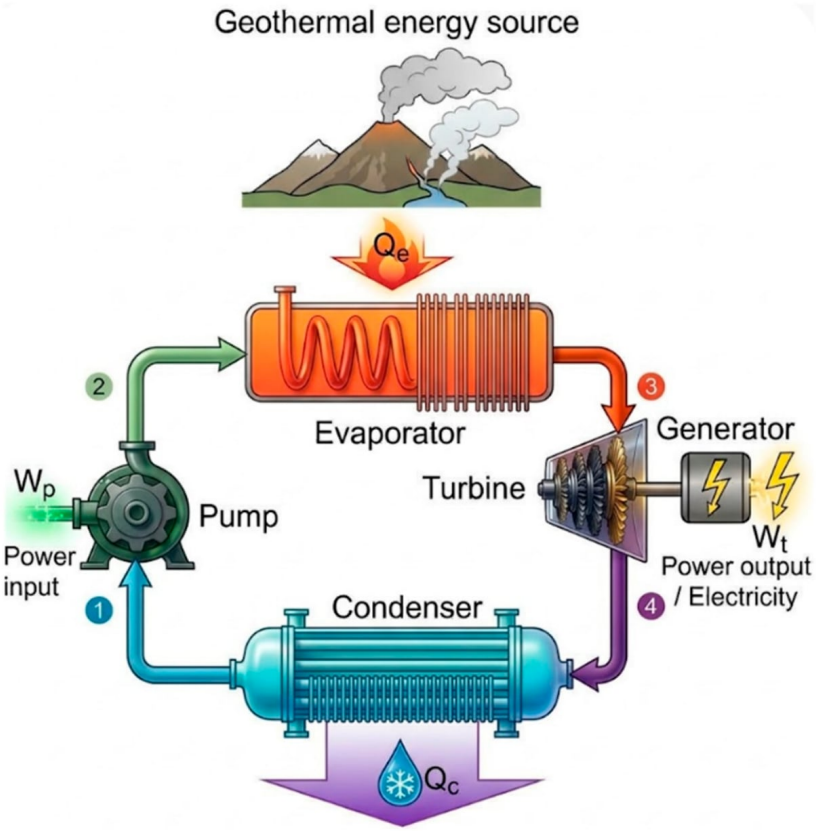


Figure 1. Electricity generation via geothermal-based Organic Rankine cycle.

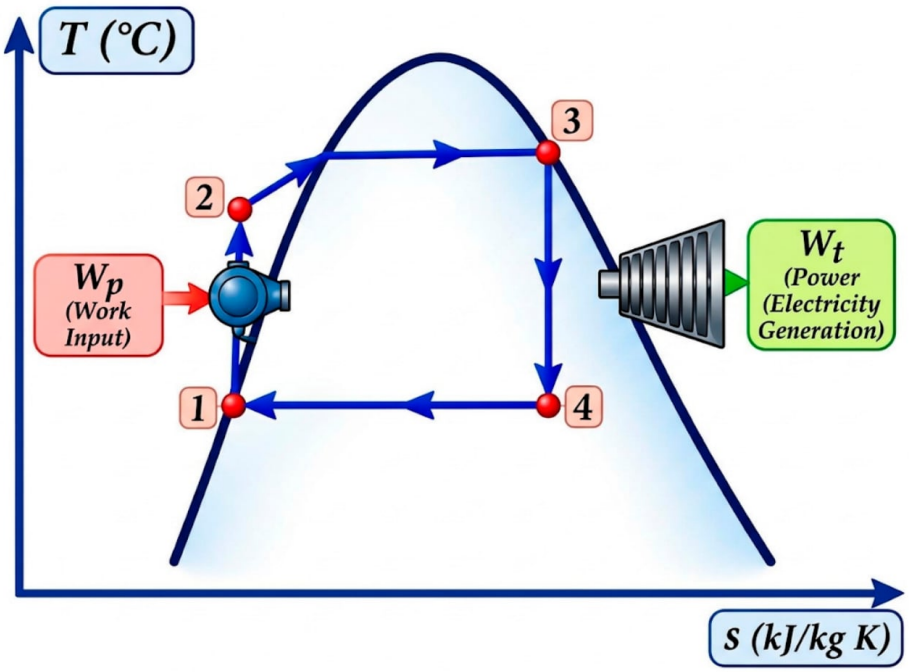


Figure 2. *T-s* diagram of the geothermal source Organic Rankine cycle.

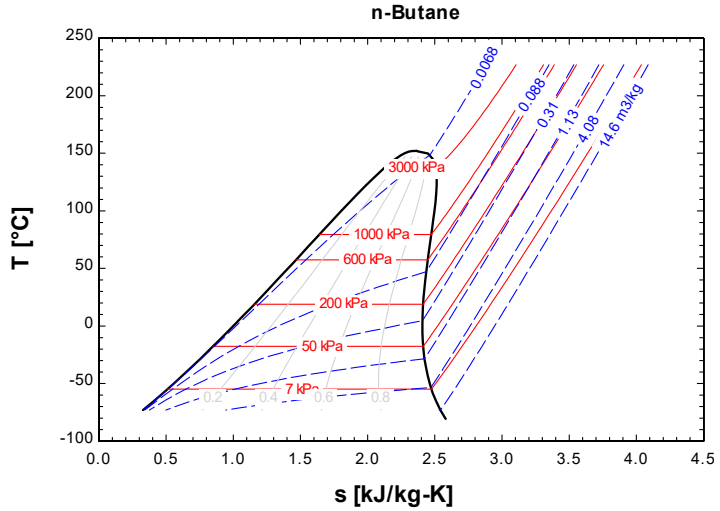


Figure 3. General *T*-*s* diagram of n-Butane.

2.2. Organic Fluid Analysis

Alternative organic working fluid mixtures were developed from pure compounds shared across the fluid libraries of EES (Klein, 2025 [30]) and REFPROP (Lemmon et al., 2018 [31]). The selection and formulation process was governed by the following criteria:

- Suitability for the designated geothermal heat source temperature range;
- Representation of diverse chemical families among the constituent pure organic fluids;
- Classification as either dry or isentropic type fluids based on the slope of their saturation vapor curves;
- Zero Ozone Depletion Potential (ODP = 0);
- Compatibility with at least one mutual lubricating oil across operating conditions.

A cycle model was established in EES for the energy and exergy evaluation of the organic mixtures designated for the geothermal ORC. Table 1 lists the primary thermophysical properties of the candidate pure fluids sourced from the REFPROP 10 library and modeled within the cycle.

Table 1. Pure organic fluids to be used for refrigerant blends and their thermophysical properties [2,30–48].

Refrigerant	T_{CR} (°C)	P_{CR} (bar)	Boiling Point (°C)	Lubricating Oil	GWP	Safety Class	Fluid Type
Hydrocarbons (HC's)							
Isobutane (R600a)	134.7	36.3	−8.8	MCO, Alkyl benzene, POE	20	A3	Dry
Butane (R600)	152	38	−0.5	POE	4	A3	Dry
İzopentan (R601a)	187.2	33.7	27.8	POE, PAO	20	A3	Dry
Pentane (R601)	196.6	33.7	36.1	POE	5	A3	Dry
Cyclopentane	238.6	45.8	49.3	POE, PAO	<5	A3	Dry
Hexane	235	30.6	69	POE	3.1	A3	Dry
Hydrofluoroolefins (HFO's)							
R1233zd(E)	166.5	36.2	18.3	POE, PAG68	1	A2L	Dry
R1224yd(Z)	156	33.4	14.6	POE	1	A2L	Dry
Hydrofluorocarbons (HFC's)							
R245fa	154	36.1	15	POE	1030	A2L	Isentropic
R236ea	139.3	35	6.2	POE	710	A1	Dry
R365mfc	186.9	34.9	40.2	POE, PAO	890	A1	Dry
R236fa	124.9	32	27.2	PAO, POE	9810	A1	Dry

Among the 108 newly generated organic mixtures, candidates with temperature glide values exceeding the targeted limit were filtered out. The remaining viable mixtures yielding the highest thermodynamic performance across the cycle were subsequently identified and are listed in Table 2.

The initial pool of pure fluids was screened by discarding wet organic fluids, followed by removing candidates incompatible with the cycle's thermodynamic model. Moreover, non-toxic, low-flammability fluids with high critical temperatures and zero ODP were chosen from the remaining pure organic candidates. Because the selected dry and isentropic organic working fluids exhibit positively sloped or nearly vertical saturated vapor curves ($ds/dT \geq 0$), the turbine exhaust stream (State 4) exits at a superheated vapor state with elevated residual thermal energy. Incorporating an internal heat exchanger (recuperator) or regenerative preheating configuration can recover this sensible superheat to preheat the compressed liquid entering the evaporator (State 2), thereby reducing external heat input requirements and enhancing cycle η_{th}. However, in geothermal power plants, recuperation simultaneously elevates the evaporator inlet temperature and raises the geothermal brine reinjection (outlet) temperature (T_{out}), creating a thermodynamic trade-off between η_{th} enhancement and total heat extraction from the brine; therefore, a basic non-recuperative ORC configuration was adopted in this study to maximize brine heat utilization across the 130–150 °C source range.

Analysis of Organic Mixtures

Based on the 10 pure fluids presented in Table 1, a total of 108 candidate organic fluid mixtures were generated using the REFPROP 10 software, following the criteria outlined below, and are presented in Table 2. The blend compositions were incremented at steps of 10% by mass. Candidate mixtures possessing a safety group classification no higher than A2L were subsequently designated as working fluids.

Table 2. Thermophysical properties of candidate organic fluid mixtures [31].

New Mixture Code	Proportions	T_{CR} (°C)	T_G (°C)	PCR (bar)	GWP	SC
B1	R601/R1336mzz(Z) (0.9/0.1)	194.5	0.4	33.5	4.7	A3
B2	R601/R1336mzz(Z) (0.8/0.2)	192.3	0.7	33.2	4.4	A3
B3	R601/R1336mzz(Z) (0.7/0.3)	189.8	0.9	33	4.1	A3
B4	R601/R1336mzz(Z) (0.6/0.4)	187.2	0.94	32.6	3.8	A3
B5	R601/R1336mzz(Z) (0.5/0.5)	184.3	0.84	32.1	3.5	A2
B6	R601/R1336mzz(Z) (0.4/0.6)	181.2	0.6	31.6	3.2	A2L
B7	R601/R1336mzz(Z) (0.3/0.7)	178.1	0.3	31	2.9	A1
B8	R601/R1336mzz(Z) (0.2/0.8)	175	0.07	30.3	2.6	A1
B9	R601/R1336mzz(Z) (0.1/0.9)	172.5	0.01	29.7	2.3	A1
B10	R600/R1234ze(Z) (0.9/0.1)	150.4	0.14	37.7	4.2	A3
B11	R600/R1234ze(Z) (0.8/0.2)	148.8	0.18	37.5	4.4	A3
B12	R600/R1234ze(Z) (0.7/0.3)	147.2	0.13	37.2	4.6	A3
B13	R600/R1234ze(Z) (0.6/0.4)	145.7	0.05	36.8	4.8	A3
B14	R600/R1234ze(Z) (0.5/0.5)	144.4	0	36.5	5	A2
B15	R600/R1234ze(Z) (0.4/0.6)	143.5	0.1	36.2	5.2	A2
B16	R600/R1234ze(Z) (0.3/0.7)	143.2	0.46	35.9	5.4	A2/A2L
B17	R600/R1234ze(Z) (0.2/0.8)	144	1.1	35.7	5.6	A2L
B18	R600/R1234ze(Z) (0.1/0.9)	146.2	1.4	35.6	5.8	A2L
B19	R600/R245fa (0.9/0.1)	148.9	2.1	38.3	106.6	A3
B20	R600/R245fa (0.8/0.2)	145.4	3	38.1	209.2	A3
B21	R600/R245fa (0.7/0.3)	141.7	2.9	37.7	311.8	A3
B22	R601/R245fa (0.6/0.4)	137.9	2	37	414.4	A3
B23	R600/R245fa (0.5/0.5)	134.6	0.6	36.3	517	A3/B1
B24	R600/R245fa (0.4/0.6)	132.4	0.1	35.6	619.6	B1
B25	R600/R245fa (0.3/0.7)	132.7	2.2	35.6	722.2	B1

Table 2. *Cont.*

New Mixture Code	Proportions	T_{CR} (°C)	T_G (°C)	PCR (bar)	GWP	SC
B26	R600/R245fa (0.2/0.8)	136.3	5.8	36.2	824.8	B1
B27	R600/R245fa (0.1/0.9)	143.6	7.6	37.1	927.4	B1
B28	R600/R236ea (0.9/0.1)	150.2	0.4	37.8	74.6	A3
B29	R600/R236ea (0.8/0.2)	148.1	0.7	37.6	145.2	A3
B30	R600/R236ea (0.7/0.3)	145.9	0.8	37.3	215.8	A3
B31	R600/R236ea (0.6/0.4)	143.5	0.7	37	286.4	A3
B32	R600/R236ea (0.5/0.5)	141	0.5	36.5	357	A2
B33	R600/R236ea (0.4/0.6)	138.4	0.2	35.9	427.6	A2L
B34	R600/R236ea (0.3/0.7)	136.1	0	35.3	498.2	A1
B35	R600/R236ea (0.2/0.8)	134.7	0.3	34.8	568.8	A1
B36	R600/R236ea (0.1/0.9)	135.3	1	34.5	639.4	A1
B37	R601/R365mfc (0.9/0.1)	193.1	2.3	33.9	93.5	A1
B38	R601/R365mfc (0.8/0.2)	189.4	3.4	33.9	182	A1
B39	R601/R365mfc (0.7/0.3)	185.4	3.5	33.6	270.5	A1
B40	R601/R365mfc (0.6/0.4)	181.4	2.6	33.2	359	A1
B41	R601/R365mfc (0.5/0.5)	177.8	1.3	32.6	447.5	A2L
B42	R601/R365mfc (0.4/0.6)	175	0.2	32.1	536	A3
B43	R601/R365mfc (0.3/0.7)	173.9	0.3	31.9	624.5	A3
B44	R601/R365mfc (0.2/0.8)	175.4	1.7	32.1	713	A3
B45	R601/R365mfc (0.1/0.9)	179.9	2.8	32.7	801.5	A3
B46	R1336mzz(Z)/R365mfc (0.9/0.1)	171.9	0	29.3	90.8	A1
B47	R1336mzz(Z)/R365mfc (0.8/0.2)	172.6	0.02	29.7	179.6	A1
B48	R1336mzz(Z)/R365mfc (0.7/0.3)	173.7	0.1	30	268.4	A1
B49	R1336mzz(Z)/R365mfc (0.6/0.4)	175	0.2	30.4	357.2	A1
B50	R1336mzz(Z)/R365mfc (0.5/0.5)	176.6	0.3	30.8	446	A2L
B51	R1336mzz(Z)/R365mfc (0.4/0.6)	178.4	0.44	31.2	534.8	A2
B52	R1336mzz(Z)/R365mfc (0.3/0.7)	180.3	0.5	31.6	623.6	A2
B53	R1336mzz(Z)/R365mfc (0.2/0.8)	182.4	0.5	32	712.4	A2
B54	R1336mzz(Z)/R365mfc (0.1/0.9)	185.4	0.4	32.3	801.2	A2
B55	R1234ze(Z)/R1233zd(E) (0.9/0.1)	150.7	0.03	35.3	5.5	A2L
B56	R1234ze(Z)/R1233zd(E) (0.8/0.2)	151.4	0.1	35.4	5	A2L
B57	R1234ze(Z)/R1233zd(E) (0.7/0.3)	152.4	0.2	35.4	4.5	A2L
B58	R1234ze(Z)/R1233zd(E) (0.6/0.4)	153.7	0.4	35.6	4	A2L
B59	R1234ze(Z)/R1233zd(E) (0.5/0.5)	155.1	0.6	35.7	3.5	A1/A2L
B60	R1234ze(Z)/R1233zd(E) (0.4/0.6)	156.9	0.7	35.8	3	A1
B61	R1234ze(Z)/R1233zd(E) (0.3/0.7)	158.9	0.8	35.9	2.5	A1
B62	R1234ze(Z)/R1233zd(E) (0.2/0.8)	161.2	0.8	36.1	2	A1
B63	R1234ze(Z)/R1233zd(E) (0.1/0.9)	163.7	0.6	36.2	1.5	A1
B64	R1234ze(Z)/R1224yd(Z) (0.9/0.1)	149.7	0	35.1	5.5	A2L
B65	R1234ze(Z)/R1224yd(Z) (0.8/0.2)	149.5	0.02	34.9	5	A2L
B66	R1234ze(Z)/R1224yd(Z) (0.7/0.3)	149.4	0.02	34.6	4.5	A2L
B67	R1234ze(Z)/R1224yd(Z) (0.6/0.4)	149.5	0.06	34.4	4	A2L
B68	R1234ze(Z)/R1224yd(Z) (0.5/0.5)	149.8	1.1	34.2	3.5	A1/A2L
B69	R1234ze(Z)/R1224yd(Z) (0.4/0.6)	150.4	0.2	34.1	3	A1
B70	R1234ze(Z)/R1224yd(Z) (0.3/0.7)	151.2	0.3	33.9	2.5	A1
B71	R1234ze(Z)/R1224yd(Z) (0.2/0.8)	152.3	0.4	33.8	2	A1
B72	R1234ze(Z)/R1224yd(Z) (0.1/0.9)	153.8	0.3	33.6	1.5	A1
B73	R1233zd(E)/R245fa (0.9/0.1)	163.7	0.6	36.3	103.9	A1
B74	R1233zd(E)/R245fa (0.8/0.2)	161.2	0.8	36.3	206.8	A1/A2L
B75	R1233zd(E)/R245fa (0.7/0.3)	158.9	0.8	36.2	309.7	A2L
B76	R1233zd(E)/R245fa (0.6/0.4)	156.9	0.6	36.1	412.6	A2
B77	R1233zd(E)/R245fa (0.5/0.5)	155.3	0.3	36.1	515.5	A2
B78	R1233zd(E)/R245fa (0.4/0.6)	154.1	0.1	36	618.4	A2/B1
B79	R1233zd(E)/R245fa (0.3/0.7)	153.4	0.02	36.1	721.3	B1
B80	R1233zd(E)/R245fa (0.2/0.8)	153.1	0	36.2	824.2	B1
B81	R1233zd(E)/R245fa (0.1/0.9)	153.3	0.03	36.3	927.1	B1
B82	R1233zd(E)/R236ea (0.9/0.1)	163.2	1.1	36.2	71.9	A1
B83	R1233zd(E)/R236ea (0.8/0.2)	159.9	1.8	36.1	142.8	A1
B84	R1233zd(E)/R236ea (0.7/0.3)	156.7	2.03	36	213.7	A1

Table 2. *Cont.*

New Mixture Code	Proportions	T_{CR} (°C)	T_G (°C)	PCR (bar)	GWP	SC
B85	R1233zd(E)/R236ea (0.6/0.4)	153.5	2	35.7	284.6	A1
B86	R1233zd(E)/R236ea (0.5/0.5)	150.5	2.3	35.5	355.5	A1
B87	R1233zd(E)/R236ea (0.4/0.6)	147.6	1.3	35.1	426.4	A1
B88	R1233zd(E)/R236ea (0.3/0.7)	145	3.8	34.8	497.3	A1
B89	R1233zd(E)/R236ea (0.2/0.8)	142.7	0.4	34.6	568.2	A1
B90	R1233zd(E)/R236ea (0.1/0.9)	140.8	0.1	34.3	639.1	A1
B91	R1224yd(Z)/R245fa (0.9/0.1)	153.6	0.4	33.7	103.9	A1
B92	R1224yd(Z)/R245fa (0.8/0.2)	151.9	0.4	33.9	206.8	A1/A2L
B93	R1224yd(Z)/R245fa (0.7/0.3)	150.7	0.3	34.1	309.7	A2L
B94	R1224yd(Z)/R245fa (0.6/0.4)	149.9	0.1	34.3	412.6	A2
B95	R1224yd(Z)/R245fa (0.5/0.5)	149.5	0.02	34.6	515.5	A2
B96	R1224yd(Z)/R245fa (0.4/0.6)	149.6	0	34.9	618.4	A2/B1
B97	R1224yd(Z)/R245fa (0.3/0.7)	150.2	0.1	35.2	721.3	B1
B98	R1224yd(Z)/R245fa (0.2/0.8)	151.1	0.1	35.6	824.2	B1
B99	R1224yd(Z)/R245fa (0.1/0.9)	152.3	0.2	36.1	927.1	B1
B100	R1224yd(Z)/R236ea (0.9/0.1)	153.8	0.4	33.5	71.9	A1
B101	R1224yd(Z)/R236ea (0.8/0.2)	152.1	0.6	33.7	142.8	A1
B102	R1224yd(Z)/R236ea (0.7/0.3)	150.3	0.7	33.8	213.7	A1
B103	R1224yd(Z)/R236ea (0.6/0.4)	148.6	0.8	33.9	284.6	A1
B104	R1224yd(Z)/R236ea (0.5/0.5)	147	0.8	34	355.5	A1
B105	R1224yd(Z)/R236ea (0.4/0.6)	145.3	0.7	34	426.4	A1
B106	R1224yd(Z)/R236ea (0.3/0.7)	143.7	0.6	34.1	497.3	A1
B107	R1224yd(Z)/R236ea (0.2/0.8)	142.2	0.4	34.1	568.2	A1
B108	R1224yd(Z)/R236ea (0.1/0.9)	140.7	0.2	34.1	639.1	A1

Thermodynamic analyses of the newly generated organic fluid blends were performed adopting the baseline assumptions outlined in Table 3. Operating conditions were established with a condenser temperature of 30 °C and geothermal heat source temperatures in the intermediate regime of 130–150 °C, incremented by 5 °C starting from 130 °C. The results generated by the EES-based geothermal ORC framework were scrutinized, and the 60 candidate mixtures demonstrating the maximum η_{th} and η_{II} metrics were determined.

Table 3. Working conditions and assumptions for Organic Rankine cycle.

$\dot{m}_{gw}$ (kg/s)	T_{con} (°C)	ΔT_{pinch} (°C)	T_{in} (°C)	T_{out} (°C)	c_{geo} (kJ/kg·°C)
30	30	15	130–150	80	4.18

Finally, from among the 60 candidate mixtures, those that showed only minor differences in their η_{th} and η_{II} metrics were eliminated; consequently, the number of organic working fluid mixtures was reduced to a final selection of 12 distinct organic fluid mixtures that yielded the best results in terms of energy and exergy analysis.

In the selection of working fluid mixtures, new organic candidate mixtures were generated using REFPROP, with components varied in 10% increments. As a first screening step, mixtures with a safety classification higher than A2L in accordance with F-Gas regulations were excluded. In the second step, candidate mixtures with a temperature glide greater than 5 °C were eliminated. This process narrowed the selection down to 60 candidate mixtures that met the A2L safety classification and had a temperature glide of less than 5 °C. From these, 12 final organic mixtures selected from the available binary combinations based on the best energy and exergy analysis results were identified as the chosen working fluids.

The organic mixtures were formulated under strict criteria: Close proximity of normal boiling points among constituent pure fluids, representation of differing refrigerant groups, availability of at least one compatible lubricant shared by the blended fluids, a temperature glide restricted to less than 5 °C, and a GWP value below 750. The novel organic fluid

blends under investigation were classified into two tiers based on environmental metrics and F-gas regulatory compliance: GWP < 150 and 150 < GWP < 750. Additionally, targeting superior energy efficiency, second-law performance, and net power generation, three critical temperature brackets were examined: T_{CR} < 150 °C, 150 °C < T_{CR} < 165 °C, and T_{CR} > 165 °C. A comparative energy and exergy evaluation was subsequently conducted among the organic fluids within each defined category.

Table 4 summarizes key properties of the selected new organic blends obtained via REFPROP 10 under baseline conditions of 25 °C and 101.3 kPa.

Table 4. Organic mixtures and thermophysical properties [31].

Blended Refrigerant	Proportions	ρ (kg/m^3)	k (mW/m K)	c_p (kJ/kg K)	μ (Pa s)	P_{CR} (kPa)	M (kg/kmol)
b1	R601/R1336mzz(Z) (0.5/0.5)	916	95	1.7	256.4	3162	108.7
b2	R600/R1234ze(Z) (0.5/0.5)	3.74	14.4	1.1	9	3588	88.5
b3	R600/R236ea (0.5/0.5)	3.9	16	1.2	9.9	3593	92.4
b4	R601/R365mfc (0.9/0.1)	651.6	109.6	2.2	222.6	3387	76
b5	R1336mzz(Z)/R365mfc (0.9/0.1)	1349.2	73.2	1.23	370.9	2934	162.3
b6	R1336mzz(Z)/R365mfc (0.8/0.2)	1335	74.3	1.25	379.6	2965	160.6
b7	R1234ze(Z)/R1233zd(E) (0.1/0.9)	5.5	10.8	0.82	10.2	3617	128.6
b8	R1234ze(Z)/R1224yd(Z) (0.9/0.1)	5	12.3	0.85	9.64	3508	116.8
b9	R1233zd(E)/R245fa (0.8/0.2)	5.6	11	0.83	10.3	3627	131.2
b10	R1233zd(E)/R236ea (0.9/0.1)	5.63	10.9	0.82	10.4	3622	132.4
b11	R1224yd(Z)/R245fa (0.9/0.1)	6.25	10.8	0.8	10.7	3366	146.9
b12	R1224yd(Z)/R236ea (0.9/0.1)	6.33	11	0.8	10.8	3353	148.8

2.3. Model of the Geothermal-Based Organic Rankine Cycle

A mathematical framework for the geothermal-powered ORC was developed in EES, followed by energy and exergy evaluations. A set of boundary conditions and operational assumptions was implemented for both the organic working medium and the geothermal fluid (Table 5). Accordingly, the condensing temperature was fixed at 30 °C, and a medium-temperature geothermal source spanning 130–150 °C was considered. These operating temperatures were specified in alignment with the thermal requirements for converting geothermal heat into electricity. Moreover, the cycle simulation relies on the following baseline assumptions:

- Isobaric conditions are assumed across both heat exchangers, maintaining equal inlet and outlet pressures for the evaporator and condenser.
- Heat transfer from the system and piping to the surroundings is ignored.
- Component and pipeline pressure losses are disregarded.
- A constant 15 °C temperature difference is defined between the geothermal water and the evaporator temperature.
- The organic working fluid exits the evaporator as a saturated vapor (x3 = 1) with zero degree of superheating ($\Delta T_{sup\ heat}$ = 0 °C), as dry and isentropic fluids inherently avoid two-phase moisture formation during turbine expansion without requiring superheat.

Table 5. Working conditions and constants.

T_{con} (°C)	T_0 (K)	P_{gs} (kPa)	η_t (-)	η_p (-)	T_{gs} (°C)	ΔT_{pinch} (°C)	c_{geo} (kJ/kg·°C)	$\dot{m}_{geo}$ (kg/s)
30	298	800	0.80	0.70	130–150	15	4.18	30

Mathematical model of the geothermal ORC:

Heat energy extracted by an ORC system from a geothermal source ($\dot{Q}_{geo}$) and heat of evaporation in the evaporator ($\dot{Q}_{ev}$) from Equation (1):

$$\dot{m}_{geo}\, c_{geo}\, (T_{in} - T_{out}) = \dot{m}_{of}\, (h_3 - h_2) \quad (1)$$

the flow rate of the organic fluid is calculated.

The power produced in the ORC turbine is obtained using Equation (2), while the power consumed by the pump is obtained using Equation (3):

$$\dot{W}_{\mathrm{t}} = \dot{m}_{\mathrm{of}} \, (h_3 - h_4) \tag{2}$$

$$\dot{W}_{\mathrm{p}} = \dot{m}_{\mathrm{of}} \, (h_2 - h_1) \tag{3}$$

The actual enthalpy values at the turbine and pump outlets of the ORC are calculated using the following equations:

$$h_4 = h_3 - (h_3 - h_{4\mathrm{s}}) \, \eta_{\mathrm{t}} \tag{4}$$

$$h_2 = h_1 + (h_{2\mathrm{s}} - h_1)/\eta_{\mathrm{p}} \tag{5}$$

The net power output of the ORC system is calculated using Equation (6), the back-work ratio is calculated Equation (7) and the amount of heat extracted from the geothermal source is calculated using Equation (8):

$$\dot{W}_{\mathrm{net}} = \left(\dot{W}_{\mathrm{t}} - \dot{W}_{\mathrm{p}}\right) \tag{6}$$

$$BWR = \left(\dot{W}_{\mathrm{p}}/\dot{W}_{\mathrm{t}}\right) \tag{7}$$

$$\dot{Q}_{\mathrm{in}} = \dot{m}_{\mathrm{geo}} \, c_{\mathrm{geo}} \, (T_{\mathrm{in}} - T_{\mathrm{out}}) \tag{8}$$

The total exergy flux entering the system is calculated using Equation (9):

$$\dot{E}_{\mathrm{in}} = \dot{m}_{\mathrm{geo}} \, ((h_{\mathrm{in}} - h_{\mathrm{out}}) - T_0 \, (s_{\mathrm{in}} - s_{\mathrm{out}})) \tag{9}$$

Thermal efficiency and second-law efficiency of a geothermal-based ORC:

$$\eta_{\mathrm{th}} = \dot{W}_{\mathrm{net}}/\dot{Q}_{\mathrm{in}} \tag{10}$$

$$\eta_{u} = \dot{W}_{\mathrm{net}}/\dot{E}_{\mathrm{in}} \tag{11}$$

2.4. Calculation of Glide Temperatures of Organic Mixtures

In zeotropic blends, the temperature difference between the bubble and dew points is defined as the temperature glide (T_G). Selecting pure fluids with closely matched normal boiling points is expected to proportionally minimize the mixture's temperature glide. The temperature glide corresponds to the difference between the condensation temperature and the evaporation temperature of the blend:

$$T_{\mathrm{Gmx}} = T_{\mathrm{dpmx}} - T_{\mathrm{bpmx}} \tag{12}$$

From a physical standpoint, temperature glide in binary zeotropic mixtures arises from the preferential vaporization and condensation behavior of constituent fluids possessing different normal boiling points and volatilities. During an isobaric evaporation process initiated at the saturated liquid state (bubble point T_{bpmx}), the more volatile component with the lower normal boiling point vaporizes preferentially, leaving the remaining liquid phase progressively enriched in the less volatile, higher-boiling-point component. Consequently, the saturation temperature rises continuously as phase change progresses until the saturated vapor state (dew point, T_{dpmx}) is reached, resulting in a non-isothermal phase-change trajectory rather than the constant-temperature plateau characteristic of pure working fluids.

2.5. Calculation of GWP Values for Organic Mixtures

The GWP values (GWP_{mx}) of the newly created organic mixtures are determined as follows [32]:

$$GWP_{mx} = x\%\ GWP_1 + y\%\ GWP_2 + z\%\ GWP_3 \quad (13)$$

Here, x, y, and z represent the concentration ratio of the pure fluid in the mixture, while GWP denotes the GWP value of that pure fluid. GWP values for the new candidate mixtures were calculated using this method, and the same fundamental approach was applied consistently throughout the entire manuscript.

2.6. Working Fluid Selection and Mixture Screening Methodology

The pure fluids that would form the mixtures were selected from among the fluids available in both EES WI, USA, and REFPROP 10 MD, USA,'s fluid libraries. The pure fluids to be eliminated and mixed were determined by ensuring that these pure fluids could work with at least one common oil and that the resulting mixtures had the lowest possible GWP. To determine the best alternative fluid mixture, binary candidate mixtures were created with 10% concentration increments. Those that did not run in the cycle were eliminated first. Then, the results generated by the EES-based geothermal ORC framework were scrutinized, and the 60 candidate mixtures demonstrating the maximum η_{th} and η_{II} metrics were determined. res were run in the cycle, and the mixtures with the highest η_{th} and η_{II} in EES WI, USA, were determined. Finally, mixtures exhibiting marginal differences in their η_{th} and η_{II} metrics were eliminated from these 60 candidates, thereby narrowing down the final selection to 12 distinct organic fluid mixtures. This selection scheme is presented in Figure 4.

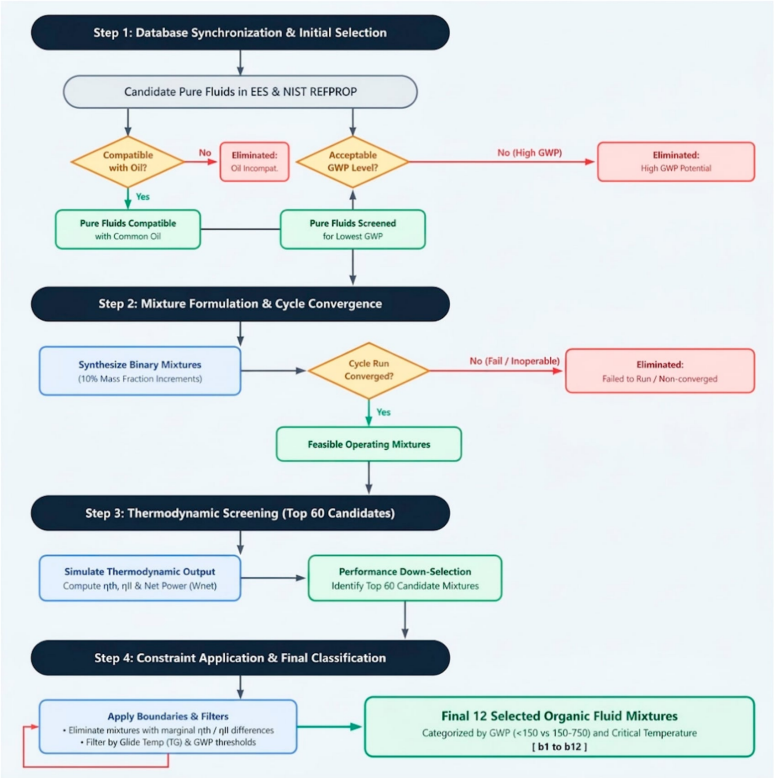


Figure 4. Organic fluid mixture selection and characterization flow chart for the geothermal source Organic Rankine cycle.

2.7. Mixture Property Analysis and Selection

The 12 novel organic fluid mixtures formulated via REFPROP were each assigned an individual code. Working fluids with GWP < 150 are grouped in Table 6 under T_{CR} < 165 °C and T_{CR} > 165 °C criteria, whereas candidate mixtures with 150 < GWP < 750 are provided in Table 7. Within Table 6, light shading indicates the T_{CR} < 165 °C group and dark shading represents the T_{CR} > 165 °C group. The corresponding GWP metrics, temperature glides, and safety ratings are also specified in the tables, sorted from highest to lowest critical temperature. The critical temperature threshold of 165 °C was selected based on the upper geothermal source temperature limit 150 °C and the natural distribution gap between b7 163.7 °C and b5 171.9 °C. Mixtures with T_{CR} < 165 °C operate in a near-critical subcritical regime with lower latent heats of vaporization and higher operating pressures, whereas mixtures with T_{CR} > 165 °C remain in a deep subcritical regime across the entire 130–150 °C heat source range.

Table 6. Some results of blended refrigerants with GWP < 150 [31].

New Blended Organic Mixture	T_{CR} (°C)	T_G (°C)	GWP	SC
b4	193.1	2.3	93.5	A1
b1	181.2	0.6	3.2	A2L
b5	171.9	0	90.8	A1
b7	163.7	0.6	1.5	A1
b10	163.2	1.1	71.9	A1
b12	153.8	0.4	71.9	A1
b11	153.6	0.4	103.9	A1
b8	149.7	0	5.5	A2L
b2	143.2	0.46	5.4	A2L

Table 7. Some results of blended refrigerants with 150 < GWP < 750 [31].

New Blended Refrigerant	T_{CR} (°C)	T_G (°C)	GWP	SC
b6	172.6	0.02	179.9	A1
b9	161.2	0.8	206.8	A1
b3	138.4	0.2	427.6	A2L

3. Results and Discussion

In practical geothermal operations, the production temperature of a geothermal reservoir does not remain strictly constant and typically experiences a gradual decline over extended operational lifetimes due to heat extraction and continuous thermal depletion of the surrounding rock matrix. For instance, a recent numerical investigation by Jia et al. demonstrated that, in closed-loop coaxial borehole heat exchangers, heat extraction induces noticeable formation thermal depletion over long-term operation, with the production temperature beginning to exhibit a discernible decline after approximately 1000 days (~2.7 years) of continuous exploitation. Nevertheless, in standard thermodynamic cycle design, optimization, and working fluid comparative screenings, it is conventional practice to treat the brine inlet state as a quasi-steady-state boundary condition. Therefore, in the present thermodynamic assessment, transient downhole reservoir dynamics and temporal thermal degradation are disregarded to systematically isolate and evaluate the intrinsic cycle performance and thermodynamic suitability of the newly formulated binary organic blends under steady-state intermediate-temperature conditions (130–150 °C). Figure 5 shows an increase in the $\dot{m}_{of}$ values as the geothermal source temperature rises for the mixtures b1, b2, b4, b5, b7, b8, and b10–b12 GWP < 150. Operating at higher $\dot{m}_{of}$ levels allows the organic working fluid to capture more thermal energy while establishing better

thermal compatibility with the geothermal brine, ultimately yielding higher heat transfer rates in the cycle.

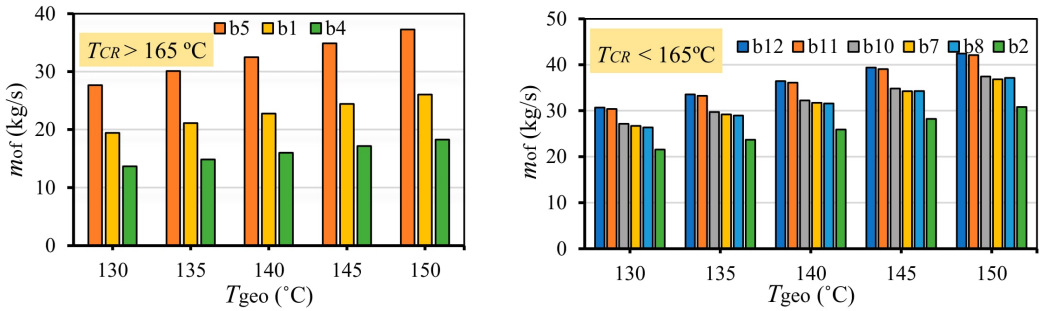


Figure 5. The variation of $\dot{m}_{of}$ with geothermal temperature for the mixtures with GWP < 150.

When evaluating the $\dot{m}_{of}$ individually, mixture b5 yielded the highest $\dot{m}_{of}$ values across the 130–150 °C geothermal source temperature range among the T_{CR} > 165 °C organic mixtures; this is attributed to its lower enthalpy of vaporization compared to the other two blends in this category and its higher molecular weight M, as evidenced by Table 3. Conversely, for the T_{CR} < 165 °C organic mixtures, the maximum $\dot{m}_{of}$ values were attained with blend b12, which likewise possesses a relatively high enthalpy difference of vaporization alongside an elevated M.

Figure 6 shows that with increasing geothermal temperature, the $\dot{W}_{net}$ values also increase for each of the mixtures with GWP < 150, namely b1, b2, b4, b5, b7, b8, and b10–b12.

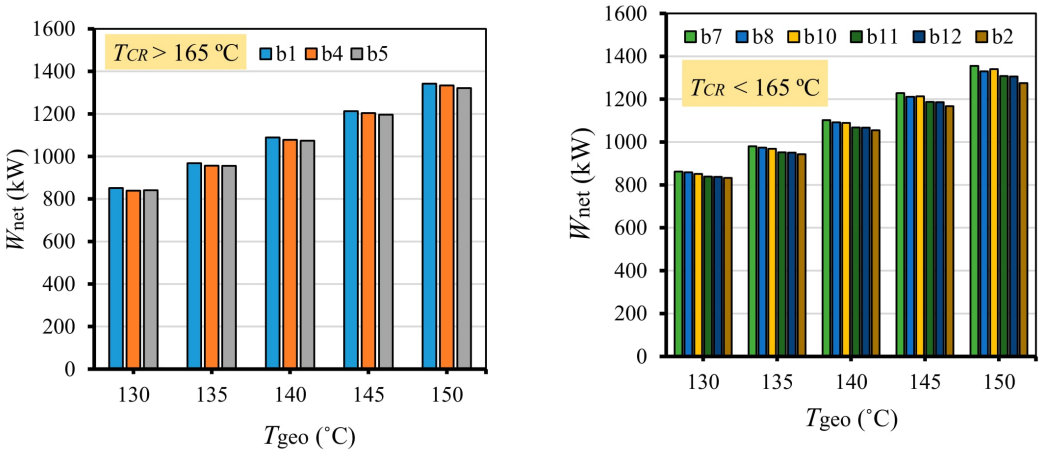


Figure 6. The effect of $\dot{W}_{net}$ on geothermal temperature for the mixtures with GWP < 150.

For all geothermal source temperatures, the maximum $\dot{W}_{net}$ is achieved by blend b1 within the T_{CR} > 165 °C category, and by blend b7 among the mixtures with T_{CR} < 165 °C. Operating in the subcritical regime, blend b1 provides an optimal evaporation pressure/temperature during saturated phase change and minimizes superheating needs, resulting in a favorable vapor density and enthalpy level entering the turbine. The leading role of b7 in its respective group is explained by high thermal compatibility, whereby optimizing the evaporator pressure enables the fluid's phase-change trajectory to align closely with the geothermal source cooling curve.

Considering the mathematical definition of $\dot{W}_{net}$ in Equation (6) the net capacity of the cycle is strictly dictated by the trade-off between the gross turbine power and the parasitic pumping load. The superiority of b7 in the sub-165 °C category stems from the concurrent

optimization of both terms. Due to the optimized evaporator operating pressure, b7 achieves an exceptional temperature profile match (thermal matching) with the geothermal cooling curve, which broadens the available expansion pressure ratio and yields a high specific turbine enthalpy drop ($h_3 - h_4$) Simultaneously, owing to its favorable liquid specific volume and balanced operating pressure levels, the enthalpy rise across the pump ($h_2 - h_1$) remains notably modest. Consequently, unlike high-mass-flow alternatives that suffer from excessive pumping penalties, b7 retains the majority of its generated turbine work, achieving the highest $\dot{W}_{net}$ via a minimized back-work ratio.

When evaluating all the $\dot{m}_{of}$ and $\dot{W}_{net}$ values collectively, a holistic evaluation of the organic fluid mass flow rate ($\dot{m}_{of}$) underscores that maximizing working fluid circulation does not inherently yield optimal thermodynamic performance. While blend b5 systematically required the highest mass flow rate across all geothermal temperatures (130–150 °C) due to its lower latent heat of vaporization, it failed to deliver the maximum power. Instead, b1 ($T_{CR} > 165$ °C) and b7 ($T_{CR} < 165$ °C) outperformed all other candidates in their respective classes. This demonstrates that net power capacity is fundamentally governed by the synergistic product of mass flow rate and specific net enthalpy drop ($\dot{m}_{of}\,\Delta\dot{W}_{net}$). Both b1 and b7 effectively mitigate parasitic pump consumption while capitalizing on superior thermal matching and expansion pressure ratios. Consequently, from both thermodynamic conversation and component sizing perspectives, b1 and b7 emerge as the most favorable candidates, offering the highest power output without the excessive hydraulic friction and equipment footprint associated with high-mass-flow mixtures like b5 [49].

To intuitively illustrate the impact of parasitic pumping consumption across all candidate mixtures, Table 8 summarizes the back-work ratio (BWR) and $\dot{W}_{net}$ across the 130–150 °C geothermal source temperature range. As the heat source temperature increases, BWR rises monotonically for every blend due to elevated operating evaporation pressures and higher circulating mass flow rates. Within the $T_{CR} > 165$ °C group, blend b1 maintains a lower BWR 0.030–0.039 than the high-mass-flow blend b5 0.031–0.041, confirming that the excessive flow rate required by b5 amplifies parasitic pumping losses and reduces its net output 841–1321kW vs. 851–1342 kW for b1. Conversely, blend b3 exhibits the highest BWR 0.083–0.120 and consequently yields the lowest $\dot{W}_{net}$ 807–1219 kW among all candidates. For the optimal low-GWP blend b7 $T_{CR} < 165$ °C, although its BWR 0.045–0.060 is slightly higher than that of b1 owing to its elevated evaporating pressure, the substantial gain in specific turbine expansion work more than compensates for the pumping load, enabling b7 to deliver the highest $\dot{W}_{net}$ 862–1355 kW across the entire evaluated temperature spectrum.

Table 8. Variations in BWR and $\dot{W}_{net}$ for geothermal resource temperature values of 130–150 °C.

	b1	b2	b3	b4	b5	b6	b7	b8	b9	b10	b11	b12
BWR (-)	0.030–0.039	0.030–0.039	0.083–0.12	0.027–0.034	0.031–0.041	0.030–0.040	0.045–0.060	0.055–0.075	0.047–0.062	0.046–0.060	0.053–0.071	0.053–0.070
W_{net} (kW)	851–1342	833–1275	807–1219	839.2–1334	841–1321	841–1320	862–1355	859–1330	854–1341	851–1340	839–1308	838–1306

As illustrated in Figure 7, η_{th} increases progressively with rising geothermal source temperature across all novel mixtures exhibiting a GWP below 150. Among the organic mixtures with $T_{CR} > 165$ °C, the highest thermal efficiency values are achieved with blend b1 at geothermal temperatures of 130 °C and 140–145 °C, with blends b4 and b5 at 135 °C, and with either b1 or b4 at 150 °C. For the candidate mixtures in the $T_{CR} < 165$ regime, the optimal thermal efficiency metrics are obtained with blend b7 at geothermal temperatures of 130 °C and 140–150 °C, and concurrently with blends b7 and b2 at 135 °C.

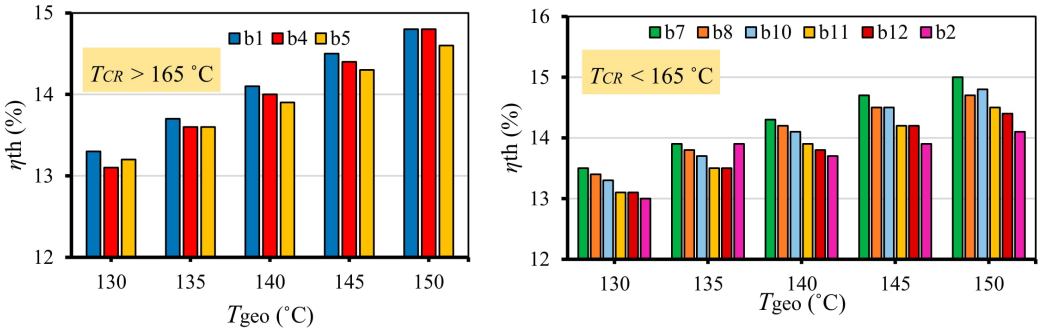


Figure 7. The variation of η_{th} with geothermal temperature for the mixtures with GWP < 150.

In terms of $\dot{W}_{net}$, the superior power yields across the entire geothermal temperature spectrum were delivered by b1 for the mixtures characterized by GWP < 150 and T_{CR} > 165 °C, and by b7 for those with GWP < 150 and T_{CR} < 165 °C (Figure 6). η_{th}, can be permanently suppressed to some extent when a high $\dot{W}_{net}$, is driven by a high $\dot{Q}_{in}$. Mixtures like b4 and b5 achieve higher η_{th} at designated temperatures because they operate with comparatively lower heat inputs. When the source temperature attains 150 °C, blend b4 rivals b1 due to a steep increase in its turbine specific enthalpy drop $(h_3 - h_4)$ with elevated evaporation pressure, coupled with a well-proportioned increase in heat intake compared to b1.

In Figure 8, η_{II} increases with rising geothermal source temperature across all novel mixtures with a GWP below 150. Among the organic working fluid mixtures characterized by GWP < 150 and T_{CR} > 165 °C, the highest η_{II} values are achieved with blend b1 across the entire geothermal temperature range of 130–150 °C (under all investigated operating conditions). For the candidate mixtures in the T_{CR} < 165 °C group, the maximum η_{II} values are consistently attained with blend b7 across all geothermal source temperatures.

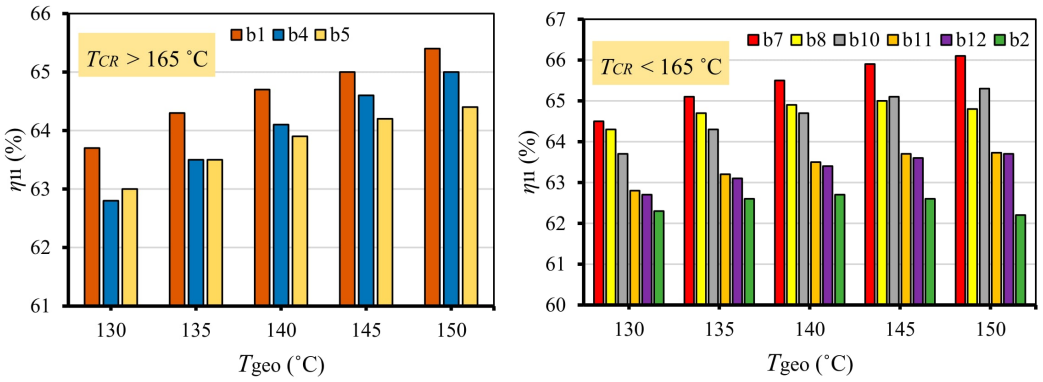


Figure 8. Change in η_{II} due to increasing geothermal temperature for GWP < 150 mixtures.

According to the evaporator energy balance $\dot{Q}_{in} = \dot{m}_{of}\ (h_3 - h_2)$, the circulating mass flow rate is inversely proportional to the specific enthalpy difference across the evaporator. Consequently, owing to their comparatively lower latent heats of vaporization and smaller enthalpy additions (Δh_{ev}) the highest $\dot{m}_{of}$ values were obtained with b5 for the T_{CR} > 165 °C group and b12 for the T_{CR} < 165 °C category across all geothermal source temperatures (Figure 4) Among the organic fluid mixtures in the T_{CR} > 165 °C group, the highest $\dot{W}_{net}$, η_{th} ve η_{II} values were achieved with blend b1, whereas for the candidate mixtures in the T_{CR} < 165 °C category, the peak values were attained with blend b7 (Figures 6–8). These comparative findings clearly demonstrate that maximizing circulating $\dot{m}_{of}$ does not directly translate into superior thermodynamic performance due to the elevated pumping power

penalties and lower latent heats associated with blends b5 and b12. Instead, b1 and b7 successfully balance the specific turbine enthalpy drop with an optimal $\dot{m}_{of}$ and minimized back-work ratio. Consequently, both mixtures simultaneously maximize $\dot{W}_{net}$, η_{th} ve η_{II} by mitigating irreversibilities in their respective critical temperature classes.

Upon inspecting Table 6 and Figure 7 to assess the effects of critical temperature and temperature glide on η_{th} and η_{II}, blend b4 presents the maximum T_{CR} among the $T_{CR} > 165$ °C organic fluid mixtures, while blend b7 yields the peak T_{CR} in the $T_{CR} < 165$ °C classification. Regarding the temperature glide, the minimum T_G is exhibited by b5 within the $T_{CR} > 165$ °C bracket, whereas b8 features the lowest T_G in the $T_{CR} < 165$ °C group. The achievement of peak η_{th} metrics with blends b1 and b7 is explained by the fundamental role of thermophysical characteristics in governing cycle efficiency. The moderate M values of b1 and b7, being lower than those of b5 and b12, facilitate an optimal operating $\dot{m}_{of}$ situated between extremes, which ultimately promotes enhanced η_{th} yields.

The suitable P_{CR} characteristics of b1 and b7 facilitated high evaporating pressures, resulting in a substantial turbine expansion ratio (P_{ev}/P_{con}). Consequently, the enlarged expansion span promoted a higher turbine enthalpy drop ($h_3 - h_4$), which augmented η_{th}. Moreover, the relatively high liquid ρ of these two blends minimized the pumping power consumption $\dot{W}_p$ for a given pressure differential. Minimizing $\dot{W}_p$, consequently improved $\dot{W}_{net}$, positively reinforcing the overall η_{th} metrics.

Owing to the fact that blend b1 yields the highest $\dot{W}_{net,}$ η_{th} ve η_{ii} values within the GWP < 150 ve $T_{CR} > 165$ °C classification, while blend b7 delivers the optimal figures for the $T_{CR} < 165$ °C group, selecting b1 for the higher critical temperature regime and b7 for the lower critical temperature bracket is suggested to attain peak energy and exergy performance.

Investigating the thermophysical characteristics of the novel mixtures indicates that b1 in the $T_{CR} > 165$ °C cohort and b7 in the $T_{CR} < 165$ °C cohort combine relatively low ρ, μ and M values with elevated k, c_p and P_{CR} metrics, thereby yielding superior η_{th} ve η_{II} results.

The parametric profiles of $\dot{m}_{of}$, $\dot{W}_{net}$, η_{th}, and η_{II} under rising geothermal source temperatures for the 150 < GWP < 750 mixtures mirrored those of the GWP < 150 group. Operating with this category resulted in a more uniform mass flow rate band (22.1–37.2 kg/s). In terms of $\dot{m}_{of}$, $\dot{W}_{net}$, the minimum power yield of the GWP < 150 tier (b2) exceeded that of the 150 < GWP < 750 tier (b3) by ~25–56 kW (~3.2–4.6%), elevating the overall lower bound. The thermal efficiencies of the 150 < GWP < 750 blends were generally lower; blend b9 yielded an η_{th} ~1.3% below the peak candidate b7. At the lower end, blend b3 delivered ~3.1–4.3% lower η_{th} than b2 across the evaluated temperatures. Similarly, the highest η_{II} attained by b9 was ~1.1% lower than that of b7, while the baseline mixture b3 (59.4–60.6%) registered an exergy efficiency ~3.0–4.5% below b2.

Geothermal fluid follows a linear cooling curve in the evaporator as it releases sensible heat; since the isothermal evaporation curves of pure fluids are incompatible with this—thereby increasing the mean temperature difference and exergy destruction—mixtures with a controlled temperature glide ($T_G < 5$ °C) offer a heating profile that runs parallel to this cooling curve, thus improving thermal matching.

When the degree of temperature glide becomes too large, the dew-point temperature at the end of evaporation (T_{dp}) approaches the geothermal inlet temperature (T_{in}) too closely, or the pinch-point location shifts from the bubble point (T_{bpmx}) toward the evaporator outlet, forcing a reduction in the evaporation pressure (P_{ev}); this, in turn, limits the turbine expansion ratio and the network output ($\dot{W}_{net}$). Furthermore, an excessive temperature glide in the condenser raises the condensation pressure, given the constraints imposed by the cooling water temperature.

Since the working fluid mixtures b1, b4, and b7—which emerged as the best options among those selected—exhibit low temperature glides, high energy and exergy efficiency values were achieved without causing a narrowing of the pinch point.

When assessing $\dot{m}_{of}$, $\dot{W}_{net}$, η_{th}, and η_{II} concurrently based on Figures 9 and 10, selecting mixture b9 is suggested to achieve superior power generation, thermal performance, and exergy efficiency within this candidate cohort.

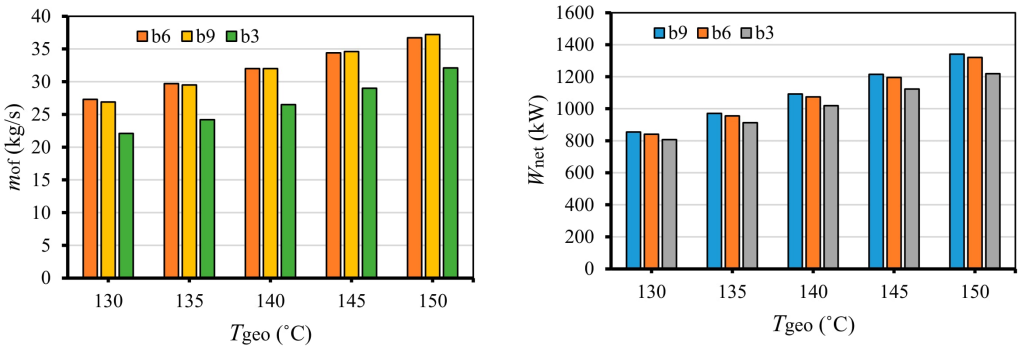


Figure 9. The variation of $\dot{m}_{of}$ and $\dot{W}_{net}$ with geothermal temperature for the mixtures with 150 < GWP < 750.

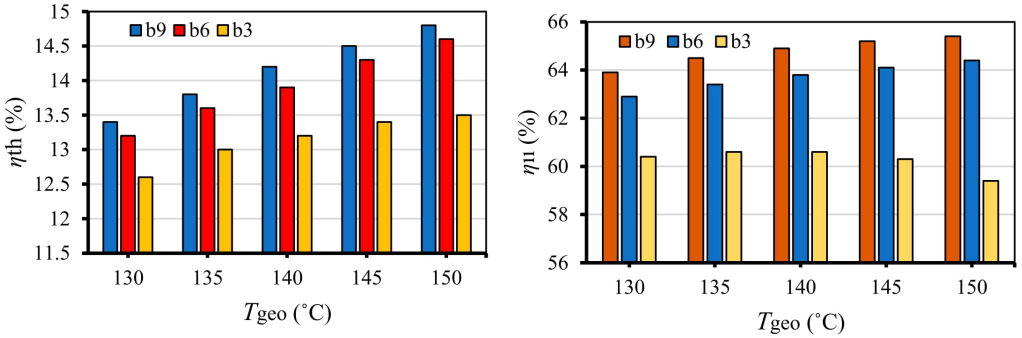


Figure 10. The dependence of η_{th} and η_{II} on geothermal temperature for the mixtures with 150 < GWP < 750.

Analogous to the results for $\dot{W}_{net}$, and η_{th}, examining the effect of critical temperature and glide on η_{II} demonstrates a variable relationship between superior η_{II} values and both T_{CR} and T_G. This confirms the deduction that fluid thermophysical properties play a vital role in determining η_{II}. Ultimately, the exergy efficiency varies as a combined function of critical temperature, temperature glide, and working fluid thermophysical parameters.

The following section provides a benchmark comparison of the current η_{th} and η_{II} metrics against previously published data from open literature employing various organic working fluids under equivalent geothermal source temperature conditions.

Model Validation

For model validation, energy and exergy analyses were conducted for 12 selected mixtures under the conditions presented in Table 9, accounting for variations in source temperature, "pinch" (temperature approach) difference, condenser temperature, and component efficiency parameters. A detailed examination of the findings revealed that the rankings of b1, b7, and b9 remained consistent, maintaining a 99% correlation even when subjected to different geothermal temperature conditions, varying pinch temperature differences, adjustments to turbine or pump efficiencies, or changes in condensation temperatures.

Table 9. Model validation data and findings.

	Working Organic Mixture	T_{gs} (°C)	ΔT_{pinch} (°C)	T_{con} (°C)	P_{in} (kPa)	η_t (-)	η_p (-)	η_{th} (-)	η_{II} (-)	$\dot{W}_{net}$ (kW)
Base Case	-	140	10	25	800	0.80	0.70	-	-	-
Test Range	-	130–150	5–15	25–45	600–800	0.70–0.90	0.60–0.80	-	-	-
Step Size	-	10	2.5	10	800	0.1	0.1	-	-	-
	b1	140	5	25	800	0.80	0.70	15.5	70.2	1181
	b2	140	5	25	800	0.80	0.70	14.8	67	1121
	b3	140	5	25	800	0.80	0.70	14.2	64.1	1078
	b4	140	5	25	800	0.80	0.70	15.4	70	1175
	b5	140	5	25	800	0.80	0.70	15.3	69.1	1162
	b6	140	5	25	800	0.80	0.70	15.3	69.1	1162
	b7	140	5	25	800	0.80	0.70	15.7	71	1194
	b8	140	5	25	800	0.80	0.70	15.4	69.8	1173
	b9	140	5	25	800	0.80	0.70	15.5	70.3	1182
	b10	140	5	25	800	0.80	0.70	15.5	70.2	1180
	b11	140	5	25	800	0.80	0.70	15.1	68.6	1153
	b12	140	5	25	800	0.80	0.70	15.1	68.5	1151
	b1	140	7.5	25	800	0.80	0.70	15.4	69.5	1169
	b2	140	7.5	25	800	0.80	0.70	14.7	66.7	1121
	b3	140	7.5	25	800	0.80	0.70	14.2	64.1	1078
	b4	140	7.5	25	800	0.80	0.70	15.3	69.1	1162
	b5	140	7.5	25	800	0.80	0.70	15.1	68.4	1151
	b6	140	7.5	25	800	0.80	0.70	15.1	68.4	1150
	b7	140	7.5	25	800	0.80	0.70	15.5	70.3	1182
	b8	140	7.5	25	800	0.80	0.70	15.3	69.3	1165
	b9	140	7.5	25	800	0.80	0.70	15.4	70	1171
	b10	140	7.5	25	800	0.80	0.70	15.4	69.5	1169
	b11	140	7.5	25	800	0.80	0.70	15	68	1143
	b12	140	7.5	25	800	0.80	0.70	15	67.9	1141
	b1	140	10	25	800	0.80	0.70	15.2	68.7	1156
	b2	140	10	25	800	0.80	0.70	14.6	66.3	1114
	b3	140	10	25	800	0.80	0.70	14.1	63.9	1074
	b4	140	10	25	800	0.80	0.70	15.1	68.1	1148
	b5	140	10	25	800	0.80	0.70	15	67.7	1139
	b6	140	10	25	800	0.80	0.70	15	67.7	1138
	b7	140	10	25	800	0.80	0.70	15.4	69.6	1170
	b8	140	10	25	800	0.80	0.70	15.2	68.7	1155
	b9	140	10	25	800	0.80	0.70	15.2	68.9	1159
	b10	140	10	25	800	0.80	0.70	15.2	68.8	1156
	b11	140	10	25	800	0.80	0.70	14.9	67.3	1132
	b12	140	10	25	800	0.80	0.70	14.9	67.2	1131
	b1	140	12.5	25	800	0.80	0.70	15	68	1143
	b2	140	12.5	25	800	0.80	0.70	14.5	66	1106
	b3	140	12.5	25	800	0.80	0.70	14	63.5	1067
	b4	140	12.5	25	800	0.80	0.70	14.9	67.4	1134
	b5	140	12.5	25	800	0.80	0.70	14.8	67	1126
	b6	140	12.5	25	800	0.80	0.70	14.8	66.9	1126
	b7	140	12.5	25	800	0.80	0.70	15.2	68.8	1157
	b8	140	12.5	25	800	0.80	0.70	15	68.1	1145
	b9	140	12.5	25	800	0.80	0.70	15.1	68.2	1146
	b10	140	12.5	25	800	0.80	0.70	15	68	1144
	b11	140	12.5	25	800	0.80	0.70	14.7	66.7	1121
	b12	140	12.5	25	800	0.80	0.70	14.7	66.6	1119
	b1	140	15	25	800	0.80	0.70	14.8	67.1	1129
	b2	140	15	25	800	0.80	0.70	14.4	65.2	1114
	b3	140	15	25	800	0.80	0.70	13.9	63	1059
	b4	140	15	25	800	0.80	0.70	14.7	66.6	1119
	b5	140	15	25	800	0.80	0.70	14.6	66.2	1113
	b6	140	15	25	800	0.80	0.70	14.6	66.2	1113
	b7	140	15	25	800	0.80	0.70	15	68	1143
	b8	140	15	25	800	0.80	0.70	14.9	67.4	1133
	b9	140	15	25	800	0.80	0.70	14.9	67.4	1133
	b10	140	15	25	800	0.80	0.70	14.8	67.2	1130
	b11	140	15	25	800	0.80	0.70	14.6	65.9	1109
	b12	140	15	25	800	0.80	0.70	14.5	65.8	1107
	b1	130	10	25	800	0.80	0.70	14.5	68.5	915.1
	b2	130	10	25	800	0.80	0.70	14.1	66.8	893
	b3	130	10	25	800	0.80	0.70	13.7	64.7	864.6

Table 9. *Cont.*

Working Organic Mixture	T_{gs} (°C)	ΔT_{pinch} (°C)	T_{con} (°C)	P_{in} (kPa)	η_t (-)	η_p (-)	η_{th} (-)	η_{II} (-)	$\dot{W}_{net}$ (kW)
b4	130	10	25	800	0.80	0.70	14.3	67.8	905.5
b5	130	10	25	800	0.80	0.70	14.3	67.6	903
b6	130	10	25	800	0.80	0.70	14.3	68	902.7
b7	130	10	25	800	0.80	0.70	14.6	69.4	927
b8	130	10	25	800	0.80	0.70	14.6	69	921.7
b9	130	10	25	800	0.80	0.70	14.5	68.8	918.9
b10	130	10	25	800	0.80	0.70	14.5	68.6	916.2
b11	130	10	25	800	0.80	0.70	14.2	67.4	900.9
b12	130	10	25	800	0.80	0.70	14.2	67.3	899.4
b1	150	10	25	800	0.80	0.70	15.8	68.7	1409
b2	150	10	25	800	0.80	0.70	14.8	64.1	1316
b3	150	10	25	800	0.80	0.70	-	-	-
b4	150	10	25	800	0.80	0.70	15.8	68.4	1403
b5	150	10	25	800	0.80	0.70	15.6	67.5	1385
b6	150	10	25	800	0.80	0.70	15.6	67.5	1384
b7	150	10	25	800	0.80	0.70	16	69.2	1421
b8	150	10	25	800	0.80	0.70	15.6	67.6	1386
b9	150	10	25	800	0.80	0.70	15.8	68.5	14.1
b10	150	10	25	800	0.80	0.70	15.8	68.5	1405
b11	150	10	25	800	0.80	0.70	15.4	67	1368
b12	150	10	25	800	0.80	0.70	15.4	66.6	1366
b1	140	10	35	800	0.80	0.70	13.8	62.5	1052
b2	140	10	35	800	0.80	0.70	13.3	60	1009
b3	140	10	35	800	0.80	0.70	12.7	57.7	970.2
b4	140	10	35	800	0.80	0.70	13.7	62	1043
b5	140	10	35	800	0.80	0.70	13.6	61.7	1037
b6	140	10	35	800	0.80	0.70	13.6	61.7	1037
b7	140	10	35	800	0.80	0.70	14	63.2	1063
b8	140	10	35	800	0.80	0.70	13.8	62.3	1048
b9	140	10	35	800	0.80	0.70	13.8	62.6	1052
b10	140	10	35	800	0.80	0.70	13.8	62.5	1051
b11	140	10	35	800	0.80	0.70	13.5	61.1	10.3
b12	140	10	35	800	0.80	0.70	13.5	61	1027
b1	140	10	45	800	0.80	0.70	12.5	56.4	948.1
b2	140	10	45	800	0.80	0.70	11.9	53.8	904.1
b3	140	10	45	800	0.80	0.70	11.4	51.6	867.4
b4	140	10	45	800	0.80	0.70	12.3	55.8	937.9
b5	140	10	45	800	0.80	0.70	12.3	55.7	936.3
b6	140	10	45	800	0.80	0.70	12.3	55.7	936.1
b7	140	10	45	800	0.80	0.70	12.6	56.9	957.5
b8	140	10	45	800	0.80	0.70	12.4	56	941.4
b9	140	10	45	800	0.80	0.70	12.4	56.3	946.6
b10	140	10	45	800	0.80	0.70	12.4	56.2	945.4
b11	140	10	45	800	0.80	0.70	12.1	55	924.2
b12	140	10	45	800	0.80	0.70	12.1	55	923.4
b1	140	10	25	800	0.70	0.70	13.2	59.9	1006
b2	140	10	25	800	0.70	0.70	12.6	57.2	962.1
b3	140	10	25	800	0.70	0.70	12.2	55	924.9
b4	140	10	25	800	0.70	0.70	13.1	59.5	1000
b5	140	10	25	800	0.70	0.70	13	58.9	991.1
b6	140	10	25	800	0.70	0.70	13	58.9	990.8
b7	140	10	25	800	0.70	0.70	13.3	60.4	1016
b8	140	10	25	800	0.70	0.70	13.1	59.5	1001
b9	140	10	25	800	0.70	0.70	13.2	59.8	1006
b10	140	10	25	800	0.70	0.70	13.2	59.7	1004
b11	140	10	25	800	0.70	0.70	12.9	58.4	981.5
b12	140	10	25	800	0.70	0.70	12.9	58.3	980
b1	140	10	25	800	0.90	0.70	17.2	77.6	13.1
b2	140	10	25	800	0.90	0.70	16.6	75.3	1266
b3	140	10	25	800	0.90	0.70	16.1	72.7	1222
b4	140	10	25	800	0.90	0.70	17	77.1	1296
b5	140	10	25	800	0.90	0.70	16.9	76.5	1286
b6	140	10	25	800	0.90	0.70	16.9	76.5	12.9
b7	140	10	25	800	0.90	0.70	17.4	78.7	13.2
b8	140	10	25	800	0.90	0.70	17.2	77.9	1310
b9	140	10	25	800	0.90	0.70	17.2	78	1312
b10	140	10	25	800	0.90	0.70	17.2	77.8	1309
b11	140	10	25	800	0.90	0.70	16.9	76.3	1283

Table 9. *Cont.*

Working Organic Mixture	T_{gs} (°C)	ΔT_{pinch} (°C)	T_{con} (°C)	P_{in} (kPa)	η_t (-)	η_p (-)	η_{th} (-)	η_{II} (-)	$\dot{W}_{net}$ (kW)
b12	140	10	25	800	0.90	0.70	16.8	76.2	1281
b1	140	10	25	800	0.80	0.60	15.1	68.4	1150
b2	140	10	25	800	0.80	0.60	14.4	65.4	1100
b3	140	10	25	800	0.80	0.60	13.9	62.9	1057
b4	140	10	25	800	0.80	0.60	15	68	1143
b5	140	10	25	800	0.80	0.60	14.9	67.4	1133
b6	140	10	25	800	0.80	0.60	14.9	67.3	1132
b7	140	10	25	800	0.80	0.60	15.2	69	1161
b8	140	10	25	800	0.80	0.60	15	68	1144
b9	140	10	25	800	0.80	0.60	15.1	68.3	11.5
b10	140	10	25	800	0.80	0.60	15.1	68.2	1147
b11	140	10	25	800	0.80	0.60	14.7	66.7	1122
b12	140	10	25	800	0.80	0.60	14.7	66.6	1120
b1	140	10	25	800	0.80	0.80	15.2	69	1160
b2	140	10	25	800	0.80	0.80	14.8	67	1125
b3	140	10	25	800	0.80	0.80	14.3	65	1086
b4	140	10	25	800	0.80	0.80	15.1	68.5	1152
b5	140	10	25	800	0.80	0.80	15	68	1143
b6	140	10	25	800	0.80	0.80	15	68	1143
b7	140	10	25	800	0.80	0.80	15.5	70	1177
b8	140	10	25	800	0.80	0.80	15.3	69.2	1164
b9	140	10	25	800	0.80	0.80	15.3	69.3	1166
b10	140	10	25	800	0.80	0.80	15.3	69.2	1163
b11	140	10	25	800	0.80	0.80	15	67.8	1140
b12	140	10	25	800	0.80	0.80	15	67.7	1138
b1	140	10	25	700	0.80	0.70	15.2	69	1156
b2	140	5	25	700	0.80	0.70	14.6	66.3	1114
b3	140	5	25	700	0.80	0.70	14.1	63.9	1074
b4	140	5	25	700	0.80	0.70	15.1	68.3	1148
b5	140	5	25	700	0.80	0.70	15	67.7	1139
b6	140	5	25	700	0.80	0.70	15	68	1138
b7	140	5	25	700	0.80	0.70	15.4	70	1170
b8	140	5	25	700	0.80	0.70	15.2	68.7	1155
b9	140	5	25	700	0.80	0.70	15.2	68.9	1159
b10	140	5	25	700	0.80	0.70	15.2	68.9	1156
b11	140	5	25	700	0.80	0.70	14.9	67.3	1132
b12	140	5	25	700	0.80	0.70	14.9	67.2	1131
b1	140	5	25	600	0.80	0.70	15.2	68.7	1156
b2	140	5	25	600	0.80	0.70	14.6	66.3	1114
b3	140	5	25	600	0.80	0.70	14.1	63.9	1074
b4	140	5	25	600	0.80	0.70	15.1	68.3	1148
b5	140	5	25	600	0.80	0.70	15	67.7	1139
b6	140	5	25	600	0.80	0.70	15	68	1138
b7	140	5	25	600	0.80	0.70	15.4	70	1170
b8	140	5	25	600	0.80	0.70	15.2	69	1155
b9	140	5	25	600	0.80	0.70	15.2	68.9	1159
b10	140	5	25	600	0.80	0.70	15.2	68.8	1157
b11	140	5	25	600	0.80	0.70	14.9	67.3	1132
b12	140	5	25	600	0.80	0.70	14.9	67.2	1131

In the table presenting the sensitivity analysis results, among the mixtures with a GWP < 150, those with a critical temperature greater than 165°C that yielded the best results are highlighted in yellow, while those with a critical temperature lower than 165°C are highlighted in green; among the mixtures with a 150 < GWP < 750, the best results are highlighted in pink.

Similarly, fixing the turbine and pump isentropic efficiencies at constant nominal values ($\eta_t = 0.80$ and $\eta_p = 0.70$) represents a standard thermodynamic screening simplification, whereas in practical ORC operation, turbomachinery efficiencies vary dynamically with volumetric flow rate, expansion/compression pressure ratio, and off-design operating regimes. Specifically, working fluids with higher molecular weights and lower latent heats of vaporization (such as b5 and b12) require substantially higher mass flow rates ($\dot{m}_{of}$) and exhibit different volumetric expansion ratios across the turbine; under real operating conditions, excessive volumetric flow variations or high pressure ratios can induce secondary flow, clearance, and partial-admission losses that shift the actual isentropic efficiency away from the nominal design point. As quantified in the sensitivity analysis in Table 9 (T_{gs} = 140 °C,

ΔT_{pinch} = 10 °C, T_{con} = 25 °C, varying η_t 0.70 and 0.90 exerts a dominant influence on cycle output, shifting η_{th} for the optimal blend b7 from 13.3% to 17.4% and $\dot{W}_{net}$, from 1016 kW to 1320 kW (± 13–15% relative to the baseline), whereas varying η_p between 60% and 80% produces a much smaller effect (η_{th} shifting from 15.2% to 15.5% and $\dot{W}_{net}$ from 1161 kW to 1177 kW due to the low liquid specific volume and modest back-work ratio of organic fluids. Crucially, across the entire tested component efficiency spectrum, the relative performance hierarchy among the mixtures remains unchanged (b7 > b1 > b9), confirming that the constant-efficiency assumption does not bias the comparative fluid selection. In real turbine operation, elevated expansion pressure ratios and thermal loads directly influence blade aerodynamic efficiency and structural integrity through coupled aerothermal-mechanical interactions [50], which causes the actual isentropic efficiency to deviate from the nominal 80% design assumption under off-design flow regimes.

As the pressure decreases, the second-law efficiency value generally shows a very slight decline. With an increase in the pinch-point temperatures, it is observed that the thermal efficiency, second-law efficiency, and net power output all decrease to some extent. Physically, neglecting frictional and local pressure drops across the heat exchangers and interconnecting pipelines overestimates the effective turbine expansion pressure ratio (P_3/P_4) and underestimates the parasitic pump work, thereby yielding slightly optimistic absolute values for $\dot{W}_{net}$, η_{th}, and η_{II} compared to real plant operation. Similarly, adopting a fixed ΔT_{pinch} of 15 °C idealizes the heat transfer process by omitting the trade-off between heat exchanger surface area (UA) and irreversibility; as shown in Table 9, raising ΔT_{pinch} from 5 °C to 15 °C lowers the evaporation pressure and increases heat transfer irreversibility, reducing η_{th} and $\dot{W}_{net}$ by approximately 4.3–4.8% (e.g., from 1194 kW to 1143 kW for blend b7 at 140 °C). Nevertheless, while these idealized assumptions shift the absolute performance magnitudes upward, they affect all candidate mixtures proportionally and do not alter the relative thermodynamic superiority ranking (b7 > b1 > b9).

As evidenced by Tables 10 and 11, previous studies considered R134a, R236fa, R245fa, and R600a as working media. The fluids examined in the literature covering 90–140 °C geothermal conditions were tested in this cycle model at the common 130–140 °C heat source temperatures, allowing for a direct comparison of thermal efficiencies. Since R134a and R236fa did not operate in the cycle at 140 °C, comparisons for this geothermal temperature were made with the remaining fluids. At 130 °C, R134a was omitted for the same reason. Based on Table 9, working with R245fa, R600a, and the novel blends b1, b7, and b9 resulted in higher η_{th} values than all fluids in that study. Likewise, Table 10 reveals that higher η_{th} values were delivered by R245fa, R600a, and mixtures b1, b7, and b9 relative to all fluids examined in the other cited work.

Table 10. Non-equivalent comparison with literature studies suggesting alternative organic mixtures to R134a, R236fa, R245fa, and R600a for 130 °C geothermal temperature [51].

Studies	T_{con} (°C)	η_t (%)	η_p (%)	T_{gs} (°C)	Organic Working Fluids/Mixtures Under Study	~η_{th} (%)
Kaynaklı et al. [37]	30	75	80	130	R134a, R236fa, R245fa, R600a	10.9, 11.5, 12.2, 13
Present study	30	80	70	130	R236fa, R245fa, R600a, b1, b7, b9	12, 13.3, 12.6, 13.3, 13.5, 13.4

An examination of the findings in Table 12 reveals that, for the same geothermal source temperatures and with the turbine isentropic efficiency value from this study compared against the turbine efficiency of the reference study, significantly higher η_{II} values are generally achieved, both for conventional organic working fluids (isobutane, R245fa, and isopentane) and for the newly developed organic mixtures (b1, b7, and b9).

Table 11. Comparison with literature studies suggesting alternative organic mixtures to R134a, R236fa, R245fa, and R600a for 140 °C geothermal temperature [51].

Studies	T_{con} (°C)	η_t (%)	η_p (%)	T_{gs} (°C)	Organic Working Fluids/Mixtures Under Study	~η_{th} (%)
Kaynaklı et al. [51]	30	75	80	130	R134a, R236fa, R245fa, R600a	11, 11.9, 12.8, 13.5
Present study	30	80	70	130	R245fa, R600a, b1, b7, b9	14, 13.1 14.1, 14.3, 14.2

Table 12. Comparison with literature study suggesting alternative organic mixtures to R227ea, Isobutane, R245fa, and Isopentane [52].

Studies	η_t (%)	η_{th} (%)	η_{II} (%)	T_{gs} (°C)	Organic Working Fluids/Mixtures Under Study
Heberle et al. [52]	75	9–15	33–46	~130–150	R227ea, Isobutane, R245fa, Isopentane
Present study	75	11.7–14	59.2–66.1	130–150	Isobutane, R245fa, Isopentane, b1, b7, b9

4. Conclusions

In the present work, selected pure organic fluids were blended at different proportions and classified. Each novel organic mixture was identified with a specific code, and the 12 selected blends were comparatively evaluated against GWP and critical temperature criteria. The main results obtained from the study indicate that:

1. Aiming to jointly maximize $\dot{W}_{net}$, η_{th} and η_{II}, distinct fluid recommendations are formulated: blend b7 stands out as the ideal working medium for low-temperature geothermal resources and waste heat conversation schemes within the ultra-low-GWP domain (GWP < 150, T_{CR} < 165 °C).
2. Blend b1 is proposed as the optimal working medium for medium-to-high-enthalpy geothermal exploitation subject to strict environmental regulations (GWP < 150, T_{CR} > 165 °C), consistently delivering the highest $\dot{W}_{net}$, η_{th}, and η_{II} across varying operating states.
3. Meanwhile, blend b9 represents the foremost candidate for commercial ORC facilities within the moderate GWP bracket (150 < GWP < 750) targeting optimal energy yield, exhibiting superior thermodynamic performance across all evaluated conditions.
4. Among all evaluated working fluids, blend b7 (GWP < 150, T_{CR} < 165 °C) achieved the overall maximum $\dot{W}_{net}$, η_{th} and η_{II}, proving to be the most promising eco-friendly organic blend owing to its favorable thermophysical properties and excellent thermal matching in the evaporator.
5. Among the high-critical-temperature mixtures (GWP < 150, T_{CR} > 165), blend b5 systematically yields the highest $\dot{m}_{of}$; thus, it emerges as an attractive option for large-scale expanders where higher throughput improves blade manufacturing feasibility and suppresses severe partial-admission losses.
6. Comprehensive robustness and sensitivity verification confirms that the performance rankings of the prime candidates (b7, b1, and b9) remain remarkably consistent (maintaining over 99% correlation) against variations in heat source temperature (130–150 °C), pinch-point temperature difference (5–15 °C), condensing temperature (25–45 °C), and component isentropic efficiencies (turbine: 0.70–0.90; pump: 0.60–0.80).
7. Incorporating realistic piping and heat exchanger pressure drops (0–5%) into the cycle model induces minor penalization on net power output due to hydraulic resistances and

secondary dissipation; nevertheless, it does not alter the thermodynamic superiority hierarchy among the candidate blends, confirming their practical operational resilience.

8. Achieving the peak $\dot{W}_{net}$, η_{th} and η_{II} performance, blend b1 is recommended for organic fluid mixtures with GWP < 150 and T_{CR} > 165 °C, and blend b7 is suggested for those satisfying GWP < 150 and T_{CR} < 165 °C.
9. In the 150 < GWP < 750 cohort, the peak $\dot{W}_{net}$, η_{th} and η_{II} results were attained using blend b9 under all investigated operating states.
10. The parametric evaluation across 130–150 °C inherently captures the operational performance degradation that an ORC plant inevitably experiences as the geothermal reservoir undergoes progressive thermal depletion over decades of continuous heat extraction, providing essential operational insights for sustainable power generation.

Funding: This research received no external funding.

Data Availability Statement: In REFPROP 10, MD, USA, new blended refrigerants were created, their thermophysical properties were determined, and these refrigerants were analyzed using a mathematical model in EES WI, USA. In this analysis, the EES WI, USA, software also retrieves fluid data from its own data library.

Acknowledgments: During the preparation of this manuscript, the author used Google Gemini (Gemini 2.5 Pro) for the purposes of assisting in the preparation and visual refinement of the figures, as well as language editing. The author has reviewed and edited the output and takes full responsibility for the content of this publication.

Conflicts of Interest: The authors declare no conflict of interest.

Abbreviations

The following abbreviations are used in this manuscript:

ARC	Auto-Refrigerating Cascade
CORC	Cascade Organic Rankine cycle
CSP	Concentrated Solar Power
c_{geo}	Specific heat of geothermal water (kJ/kg °C)
DFT	Density Functional Theory
EES	Engineering Equation Solver
$\dot{E}_{in}$	Rate of Exergy Destruction (kJ/s)
FC-MDPORC	The flash cycle-modified dual-pressure Organic Rankine cycle
GWP	Global Warming Potential
h_1	Pump inlet enthalpy (kJ/kg)
h_2	Pump outlet enthalpy (kJ/kg)
h_{2s}	Isentropic pump outlet enthalpy (kJ/kg)
h_3	Evaporator outlet enthalpy (kJ/kg)
h_4	Condenser inlet enthalpy (kJ/kg)
h_{4s}	Isentropic condenser inlet enthalpy (kJ/kg)
h_{in}	Geothermal inlet enthalpy (kJ/kg)
h_{out}	Geothermal outlet enthalpy (kJ/kg)
HC	Hydrocarbon
HFC	Hydrofluorocarbon
HFO	Hydrofluoroolefin
HST	Heat source temperature
k	Heat conduction coefficient (W/m K)
M:	Molar weight (kg/kmol)
MF:	Mass fraction
MCO	Motor Cycle Engine Oil
$\dot{m}_{geo}$	Geothermal source fluid rate (kg/s)

$\dot{m}_{of}$	Organic working fluid rate (kg/s)
ODP	Ozone Depletion Potential
ORC	Organic Rankine Cycle
OTEC	Ocean thermal energy conversation
PSO	Particle Swarm Optimization
P_{CR}	Critical pressure (bar)
P_{gs}	Geothermal source pressure (kPa)
PAG	Polyalkylene Glycol
PAO	Polyalpha Olefin
POE	Polyester
RC	Rankine Cycle
ReaxFF MD	Reactive force field molecular dynamics
R-ORC	Regenerative Organic Rankine Cycle
RR-ORC	Reheat-regenerative Organic Rankine Cycle
$\dot{Q}_{con}$	Condenser heat energy (kW)
$\dot{Q}_{ev}$	Evaporator heat energy (kW)
$\dot{Q}_{geo}$	Geothermal heat input (kW)
$\dot{Q}_{in}$	Heat extracted from geothermal source (kW)
SC	Security class
SSH	Self superheater
s_{in}	Geothermal source inlet entropy (kj/kg K)
s_{out}	Geothermal source outlet entropy (kj/kg K)
T_{bpmx}	Evaporation temperature of the mixture (°C)
T_{con}	Condenser temperature (°C)
T_{CR}	Critical temperature (°C)
T_{dpmx}	Condensation temperature of the mixture (°C)
T_{ev}	Evaporator temperature (°C)
T_{G}	Glide temperature (°C)
T_{Gmx}	Glide temperature of the new mixture (°C)
T_{gs}	Geothermal source temperature (°C)
T_{0}	Ambient temperature (K)
$\Delta T_{sup\ heat}$	Superheat change in the evaporator (°C)
$\dot{W}_{net}$	Network output (kW)
$\dot{W}_{p}$	Pump power consumption (kW)
$\dot{W}_{t}$	Turbine power generation (kW)
WFFQ	Working fluid filling quantities
WHR	Waste Heat Recovery
ρ	Density (kg/m^3)
ρ_{f}	Fluid density (kg/m^3)
η_{u}	Second-law efficiency (-)
η_{p}	Pump efficiency (-)
η_{t}	Turbine efficiency (-)

References

1. Ali, Q.; Anwar, S.; Khan, M.T.I.; Yaseen, M.R.; Ashfaq, M. Estimation of economic, environmental, and social efficiency for sustainable development in G-8 and SAARC countries: A data envelopment analysis. *Environ. Sci. Pollut. Res.* **2023**, *30*, 26819–26842. [CrossRef] [PubMed]
2. Özçelik, M.; Devecioğlu, A.G.; Oruç, V. Assessment of the usability of low-GWP blended refrigerants for water-source heat pumps. *Energies* **2026**, *19*, 1534. [CrossRef]
3. Abdulrazzaq, O.A.; Mutlaq, A.A.; Kadhim, Z.A.; Khadim, B.J.; Abdullah, S.S. An overview of recent advances in geothermal energy utilization from traditional applications to low-carbon hybrid systems. *Energy* **2026**, *360*, 100054.
4. Desai, N.B.; Orozova-Bekkevold, I.M.; Christensen, F.L.; Haglind, F. Integrated assessment of geothermal energy reservoir and organic Rankine cycle systems. *Renew. Energy* **2026**, *256*, 124683. [CrossRef]
5. Shi, H.; Wang, G.; Zhang, W.; Ma, F.; Lin, W.; Ji, M. Predicting the potential of China's geothermal energy in industrial development and carbon emission reduction. *Sustainability* **2023**, *15*, 7508. [CrossRef]

6. Özçelik, M. Atık Isı Geri Kazanımlı Bir Reküperatörlü Organik Rankine Çevriminin Enerji Ve Ekserji Analizi. In Proceedings of the 8th International Thales Congress on Life, Engineering, Architecture, and Mathematics, Cairo, Egypt, 18–20 July 2026; pp. 395–396. [CrossRef]
7. Özçelik, M. Thermodynamic Investigation of Recuperative Organic Rankine Cycles for Waste Heat Recovery. In *Advanced Materials and Engineering: Characterization, Modeling, And Emerging Applications*; İlhan, M., Ed.; Bzt Turan Publishing House: Delaware, DE, USA, 2026; pp. 97–112. [CrossRef]
8. Özçelik, M. Trilateral Çevrim ve Organik Rankine Çevrimini Kullanan Birleşik Güç Sisteminin Termodinamik Analizi. Master Thesis, Konya Thecnical University, Konya, Türkiye, 2020. Available online: https://gcris.ktun.edu.tr/server/api/core/bitstreams/47dcbf50-cadf-4644-8975-9d25f3234f63/content (accessed on 22 October 2026).
9. Özçelik, M.; Bilir Sağ, N. Optimum Working Fluid Selection of Tlc-Orc Combined Power System. In Proceedings of the 3rd International Conference on Innovative Studies of Contemporary Sciences (TOKYO SUMMIT-3), Tokyo, Japan, 19–21 February 2021; pp. 375–382. Available online: https://d03ccf26-a7d6-4629-8a98-37150e445206.filesusr.com/ugd/614b1f_b25b0b668c06483eb84ad85a5ffdf359.pdf (accessed on 21 October 2026).
10. Özçelik, M.; Bilir Sağ, N. Investigation of the Combined Tlc–Orc and the Combined Orc–Orc Power System. In Proceedings of the ICENTE'19, Konya, Türkiye, 25–27 October 2019; pp. 353–357. Available online: https://icente.selcuk.edu.tr/docs/icente2019_abstract_book.pdf (accessed on 17 October 2026).
11. Bilir Sağ, N.; Özçelik, M. Trilateral Çevrim-Organik Rankine Çevrim (Tlç-Orç) ve Organik Rankine Çevrim-Organik Rankine Çevrim (Orç-Orç) Birleşik Güç Sistemlerinin Karşılaştırmalı Performans Analizi. *Konya J. Eng. Sci.* **2021**, *9*, 647–665. [CrossRef]
12. Özçelik, M.; Bilir Sağ, N. Optimum Working Fluid Selection for Orc-Orc Combined Power System. In Proceedings of the ISSRIS'21 (International Symposium of Scientific Research and Innovative Studies), Balıkesir, Türkiye, 22–25 February 2021; pp. 1059–1071. Available online: https://813e2aa8-714f-4d41-90ec-13bf6ce2b13e.filesusr.com/ugd/1dd905_e5f684e40cc248829ffe6e7a12eab0c4.pdf (accessed on 23 October 2026).
13. Ortega-Sarceda, A.; Arce, A. Impact of superheat and reheat on the thermal efficiency of Regenerative Organic Rankine Cycle (R-ORC) with optimized operating conditions. *Energy* **2026**, *360*, 141782. [CrossRef]
14. Safari, H.; Soltani, M.; Dusseault, M.B. Cascade organic rankine cycle integrated with a cogeneration system for data center backup power: Design and thermodynamic analysis. *Energy Rep.* **2026**, *16*, 109429. [CrossRef]
15. Wijayanta, A.T.; Zolfagharroshan, M.; Tareen, M.S.K.; Liaw, K.L.; Xu, M.; Zueter, A.F.; Sasmito, A.P. Electricity generation from retrofitted abandoned oil and gas wells using a geothermal-driven organic rankine cycle. *Appl. Energy* **2026**, *421*, 128198. [CrossRef]
16. Aryanfar, Y.; Wu, W. Energy and exergy analysis of a double-flash geothermal-based organic Rankine cycle system. *Renew. Energy* **2026**, *260*, 125187. [CrossRef]
17. Rahaman, M.; Islam, M.A.; Miyara, A. Energy and exergy analysis of Organic Rankine Cycles for six low-GWP refrigerants. *Next Chem. Eng.* **2026**, *2*, 100021. [CrossRef]
18. Braimakis, K.; Mikelis, A.; Charalampidis, A.; Karellas, S. Exergetic performance of CO_2 and ultra-low GWP refrigerant mixtures as working fluids in ORC for waste heat recovery. *Energy* **2020**, *203*, 117801. [CrossRef]
19. Aryanfar, Y.; Wu, W. Energy and exergy analysis of geothermal–ORC hybrid trigeneration system with a self-superheater using low-GWP working fluids. *Renew. Energy* **2026**, *275*, 126231. [CrossRef]
20. Elahi, A.E.; Mahmud, T.; Alam, M.; Hossain, J.; Biswas, B.N. Exergy analysis of organic Rankine cycle for waste heat recovery using low GWP refrigerants. *Int. J. Thermofluids* **2022**, *16*, 100243. [CrossRef]
21. Hamzaoui, M.; Grine, A.; Bendaoud, L.A.; Nesreddine, H.; Liamini, M. Theoretical analysis of a low-grade thermal energy based organic Rankine cycle coupled to an ultra-low temperature auto-cascade refrigeration cycle. *Therm. Sci. Eng. Prog.* **2026**, *75*, 104791. [CrossRef]
22. Liu, R.; Liu, C.; Luo, X.; Liu, J.; Li, J.; Xu, W.; Xin, L. Mechanism of CO_2-regulated pyrolysis behavior and thermal stability enhancement of zeotropic R1243zf mixture for organic rankine cycle. *Energy* **2026**, *342*, 139754. [CrossRef]
23. Wang, Z.; Zhang, R.; Shao, H.; Nie, T. Thermodynamic performance of flash-dual-pressure organic Rankine cycle system for power generation from hot dry rock geothermal resources. *Appl. Therm. Eng.* **2025**, *281*, 128603. [CrossRef]
24. Sanchez, F.D.; Montes, C.M.; Salvador, J.B.; Herrera, D.C. Maximizing energy yield in organic Rankine cycles powered by variable renewable sources using Low-GWP zeotropic mixtures: A dynamic off-design optimization approach. *Energy* **2026**, *360*, 141752. [CrossRef]
25. Sun, J.; Peng, B. Experimental study on the off-design operating characteristics of an organic Rankine cycle system using a zeotropic mixture. *Case Stud. Therm. Eng.* **2026**, *81*, 107985. [CrossRef]
26. F-Gas Applications in Turkey and the Kigali Amendment. Available online: https://webdosya.csb.gov.tr/db/ozonturkiye/icerikler/ozon-panel–ufe-20210407162849.pdf (accessed on 28 January 2026).
27. Laghari, A.S.; Chandio, M.W.; Kumar, L.; Assad, M.E.H. Thermodynamic Performance Analysis of Geothermal Power Plant Based on Organic Rankine Cycle (ORC) Using Mixture of Pure Working Fluids. *Energy Eng.* **2024**, *121*, 2023–2038. [CrossRef]

28. Krempus, D.; Bahamonde, S.; Stelt, T.P.V.D.; Klink, W.; Colonna, P.; Servi, C.M.D. On mixtures as working fluids of air-cooled ORC bottoming power plants of gas turbines. *Appl. Therm. Eng.* **2024**, *236*, 121730. [CrossRef]
29. Lu, P.; Chen, K.; Luo, X.; Wu, W.; Liang, Y.; Chen, J.; Chen, Y. Experimental and simulation study on a zeotropic ORC system using R1234ze(E)/R245fa as working fluid. *Energy* **2024**, *292*, 130453. [CrossRef]
30. Klein, S.A. *Engineering Equation Solver (Version 11.986)*; F-Chart Software: Madison, WI, USA, 2025.
31. Lemmon, E.W.; Bell, I.H.; Huber, M.L.; McLinden, M.O. *NIST Standard Reference Database 23: Reference Fluid Thermodynamic and Transport Properties-REFPROP, Version 10.0*; Standard Reference Data Program; National Institute of Standards and Technology: Gaithersburg, MD, USA, 2018.
32. Mohammed, H.S.K.; Srinivas, K.; Dasari, K.R. Yellapragada Naga Venkata Sai Ram Theoretical exploration of low GWP refrigerant mixtures as replacement to HFC-134A in a vapour compression refrigeration system. *J. Therm. Eng.* **2023**, *9*, 912–920. [CrossRef]
33. Fernández-Moreno, A.; Mota-Babiloni, A.; Giménez-Prades, P.; Navarro-Esbrí, J. Optimal refrigerant mixture in single-stage high-temperature heat pumps based on a multiparameter evaluation. *Sustain. Energy Technol. Assess.* **2022**, *52*, 101989. [CrossRef]
34. Liu, B.; Yang, Z.; Zhang, Y.; Lv, Z.; Chen, Y.; Chen, S. Evaluation of a low-GWP and nonflammable blend as a new alternative for R134a in the heat pump system. *Int. J. Refrig.* **2022**, *143*, 1–10. [CrossRef]
35. Polis, M.; Barta, R.B.; Thomas, C.; Hessen, U. Experimental investigation of a heat pump tumble dryer with a zeotropic refrigerant mixture. *Int. J. Refrig.* **2024**, *158*, 190–201. [CrossRef]
36. Atmaca, A.U.; Erek, A.; Ekren, O.; Çoban, M.T. Thermodynamic Performance of the Transcritical Refrigeratıon Cycle with Ejector Expansion for R744, R170, and R41. *J. Therm. Sci. Technol.* **2018**, *38*, 111–127.
37. F-Gas Properties. Available online: http://www.ethermo.us (accessed on 25 January 2026).
38. Lee, A.J.; Bach, C.K.; Bradshaw, C.R. An experimental data-driven charge model for round-tube-plate-fin heat exchangers using low-GWP refrigerants. *Int. J. Refrig.* **2024**, *158*, 405–421. [CrossRef]
39. Wu, D.; Hu, B.; Wang, R.Z. Vapor compression heat pumps with pure Low-GWP refrigerants. *Renew. Sustain. Energy Rev.* **2021**, *138*, 110571. [CrossRef]
40. Zhang, Z.; Hou, K.; Fang, L.; Wang, S.; Liu, X.; He, M. Vapor-liquid equilibrium measurements of ionic liquid [DEME][TFSI] with different hydrofluorocarbon refrigerants R152a, R32, and R143a. *Fluid Phase Equilibria* **2024**, *579*, 114022. [CrossRef]
41. Tesse, R.; Serio, M.D.; Gargiulo, R.; Basile, G.; Bragante, L.; Santacesaria, E. Vapour–liquid equilibrium measurements for binary mixtures of R32, R143a, R134a and R125 with a perfluoropolyether lubricant. *J. Fluor. Chem.* **2003**, *121*, 15–22. [CrossRef]
42. F-Gas Properties. Available online: https://www.climalife.galco.be (accessed on 20 January 2026).
43. Yang, J.; Lee, D.; Lee, S.; Han, C.; Kim, Y. Condensation heat transfer characteristics and generalized correlations of R404A, R448A, and R454C in a plate heat exchanger. *Int. Commun. Heat Mass Transf.* **2023**, *147*, 106975. [CrossRef]
44. Sun, Y.; Wang, S.; Zheng, H.; Wang, X.; He, M. Solubilities of R-1233zd(E) in Three Lubricating Oils and Impact of Oil Retention on the Evaporator Performance. *Thermophys. Thermochem. Prop.* **2024**, *69*, 1832–1841. [CrossRef]
45. Özçelik, M. Zeotropik Karışımların Kullanıldığı Jeotermal Kaynaklı Bir Organik Rankine Çevriminin Performans Değerlendirmesi. In Proceedings of the 25th International Istanbul Scientific Research Congress on Life, Engineering, Architecture, and Mathematical Sciences, Istanbul, Türkiye, 23–25 May 2026; pp. 1320–1329. [CrossRef]
46. Marchetto, D.B.; Costa, A.G.; Ferreira, A.E.L.; Ribatski, G. Flow boiling heat transfer of R1336mzz(Z) and R245fa at high saturation temperatures in small diameter horizontal channels. *Int. J. Heat Mass Transf.* **2026**, *258*, 128269. [CrossRef]
47. Jiang, S.; Liu, Z.; Zhang, X.; Hu, B. Methodology for minimum superheat degree in high temperature heat pumps: Exemplified by quasi-two-stage compression system. *Energy Convers. Manag.* **2026**, *365*, 121756. [CrossRef]
48. Araya, S.; Wemhoff, A.P.; Jones, G.F.; Fleischer, A.S. An experimental study of an Organic Rankine Cycle utilizing HCFO-1233zd(E) as a drop-in replacement for HFC-245fa for ultra-low-grade waste heat recovery. *Appl. Therm. Eng.* **2020**, *180*, 115757. [CrossRef]
49. Ma, T.; Du, C.; Gu, Z.; Lin, W.; Zeng, Y.; Zhou, J.; Yi, Y.; Yao, N.; Qian, L.; Shi, L.; et al. Diagnosing the cold start failure of fuel cell system: End-plate cell's thermo-hydraulic imbalance and its mitigation through loading control. *Chem. Eng. J.* **2026**, *538*, 176737. [CrossRef]
50. Mou, X.; Fan, J.; Zhang, J.; Duan, P. Porosity-driven aerothermal-mechanical coupling for high-performance transpiration-cooled turbine blades. *Case Stud. Therm. Eng.* **2026**, *85*, 108359. [CrossRef]
51. Kaynaklı, Ö.; Bademlioğlu, A.H.; Yamankaradeniz, N.; Yamankaradenik, R. Thermodynamıc Analysıs of the Organic Rankine Cycle and the Effect of Refrigerant Selection on Cycle Performance. *Int. J. Energy Appl. Technol.* **2017**, *4*, 101–108. Available online: https://dergipark.org.tr/en/pub/ijeat/article/318768 (accessed on 19 October 2026).
52. Heberle, F.; Brüggemann, D. Exergy based fluid selection for a geothermal Organic Rankine Cycle for combined heat and power generation. *Appl. Therm. Eng.* **2010**, *30*, 1326–1332. Erratum in *Appl. Therm. Eng.* **2011**, *31*, 3092. [CrossRef]

Disclaimer/Publisher's Note: The statements, opinions and data contained in all publications are solely those of the individual author(s) and contributor(s) and not of MDPI and/or the editor(s). MDPI and/or the editor(s) disclaim responsibility for any injury to people or property resulting from any ideas, methods, instructions or products referred to in the content.